Biophysical Journal
Article

Biophysical Society

Mesoscale Liquid Model of Chromatin Recapitulates Nuclear Order of Eukaryotes

Rabia Laghmach,[1] Michele Di Pierro,[2] and Davit A. Potoyan[1,3,4,*]
[1]Department of Chemistry, Iowa State University, Ames, Iowa; [2]Center for Theoretical Biological Physics, Rice University, Houston, Texas; [3]Department of Biochemistry and Molecular Biology and [4]Bioinformatics and Computational Biology Program, Iowa State University, Ames, Iowa

ABSTRACT The nuclear envelope segregates the genome of Eukaryota from the cytoplasm. Within the nucleus, chromatin is further compartmentalized into architectures that change throughout the lifetime of the cell. Epigenetic patterns along the chromatin polymer strongly correlate with chromatin compartmentalization and, accordingly, also change during the cell life cycle and at differentiation. Recently, it has been suggested that subnuclear chromatin compartmentalization might result from a process of liquid-liquid phase separation orchestrated by the epigenetic marking and operated by proteins that bind to chromatin. Here, we translate these observations into a diffuse interface model of chromatin, which we named the mesoscale liquid model of nucleus. Using this streamlined continuum model of the genome, we study the large-scale rearrangements of chromatin that happen at different stages of the growth and senescence of the cell and during nuclear inversion events. In particular, we investigate the role of droplet diffusion, fluctuations, and heterochromatin-lamina interactions during nuclear remodeling. Our results indicate that the physical process of liquid-liquid phase separation, together with surface effects, is sufficient to recapitulate much of the large-scale morphology and dynamics of chromatin along the life cycle of cells.

SIGNIFICANCE Eukaryotic chromatin occupies a few micrometers of nuclear space while remaining dynamic and accessible for gene regulation. The physical state of nuclear chromatin is shaped by the juxtaposition of complex, out-of-equilibrium processes on one hand and the intrinsic polymeric aspect of the genome on the other. Recent experiments have revealed a remarkable ability of disordered nuclear proteins to drive liquid-liquid phase separation of chromatin domains. We have built a mesoscale liquid model of nuclear chromatin that allows dissecting the contribution of liquid behavior of chromatin to nuclear order of eukaryotes. Our results show that liquid-liquid phase separation, together with surface effects, is sufficient for recapitulating large-scale morphology and dynamics of chromatin at many stages of the nuclear cycle.

INTRODUCTION

Functional compartmentalization is a ubiquitous hallmark of life; by segregating biomolecules and their interactions, cells achieve specialization and improved efficiency of many of their functions (1,2). In eukaryotic cells, the genetic material is separated from the cytoplasm by the nuclear membrane within a few cubic micrometers of nuclear space. Within the nuclear boundary, we find further compartmentalization that, however, exists in the absence of membranes (3). The structural organization of chromosomes changes with the cell type and phase of life, and chromosomal loci have been observed to move across genomic compartments during cell differentiation (4–6). As a consequence, chromatin compartmentalization is believed to play a role in gene regulation, stochastic cell fate determination (7,8), and the establishment of stable cellular phenotypes (9,10).

The first evidence of chromatin subnuclear organization in interphase was the discovery of the nucleolus in the early 19th century, followed by the discovery of regions in the nucleus with distinct optical properties, which were named heterochromatin and euchromatin (11). Heterochromatin appears dense and slow-diffusing, containing regions of chromosomes corresponding to mostly silenced genes. Euchromatin, on the other hand, appears less dense and more mobile, composed of mostly active genes (12,13). The latest electron microscopy tomography experiments have confirmed the DNA density variations between

Submitted June 18, 2019, and accepted for publication September 11, 2019.
*Correspondence: potoyan@iastate.edu
Editor: Tamar Schlick.
https://doi.org/10.1016/j.bpj.2019.09.013
© 2019 Biophysical Society.

heterochromatic and euchromatic regions without, however, finding any structural difference between the two types of chromatin (14).

Clear evidence of hierarchical compartmentalization in chromatin at multiple scales has emerged through studies employing DNA-DNA proximity ligation assays. First, two genomic compartments were observed (3), named A and B, which were then refined through higher-resolution experiments to reveal the existence of even smaller subcompartments (10). The A and B compartments appear to be enriched in epigenetic markings correlating with transcriptional activation and silencing, respectively. Several studies have suggested that chromatin compartmentalization may result from a process of liquid-liquid phase separation orchestrated by the epigenetic markings, which collectively act to remodel chromosomal loci (15–19). The epigenetically driven phase-segregation events appear to emerge right at the nucleosome resolution mediated by protein binding, as has been shown in the works by Bascom et al. (20–22) and Macpherson et al. (23).

Chromatin compartmentalization is also consistent with recent experiments that have revealed the remarkable ability of intrinsically disordered proteins to phase-separate and form liquid-like protein-rich droplets (24–27). Akin to oil droplets in a well-shaken bottle of vinaigrette, the protein-rich droplets can appear and disappear according to external triggers, as well as divide and undergo fusion by forming larger droplets (28–30). Most importantly, in the latest series of experiments, members of heterochromatin protein 1 family (HP1), known for regulation of heterochromatin content in the nucleus, have been shown to drive liquid-liquid phase separation both in vivo and in vitro (31,32). Consequently, protein-induced phase separation of chromosomal domains might constitute a direct physical mechanism for regulating genetic processes in space and time in the nucleus (24,33).

The global architecture of chromosomes indeed appears to be determined by the interplay between chromatin phase separation and motor activity (15–17,34,35). Besides chromatin compartmentalization, the other prominent feature of three-dimensional genome architecture, the topologically associated domains, also appears to arise through phase separation and DNA extrusion (36). Theoretical models based on polymer dynamics have been successfully used to connect one-dimensional epigenetic information to the three-dimensional architecture of the genome. Indeed, it is possible to predict the structural ensembles of human chromosomes with high accuracy relying exclusively on the information extracted from chromatin immunoprecipitation sequencing (16). The same theoretical framework, composed exclusively of polymer connectivity, motor activity, and microphase separation, was shown to successfully explain a wide range of experimental observations about the dynamics of chromosomal loci (17). The subdiffusive behavior of chromatin, together with the heterogeneity of the individual diffusing trajectories (37), the viscoelasticity of the nuclear environment (38), and the coherent motion of DNA observed by correlation spectroscopy (39), was all naturally predicted through theoretical and computational modeling.

Here, we set out to investigate the specific contribution of liquid-liquid phase separation to genome architecture and separate its effects from those of polymer connectivity and motor activity. To gain insights into the roles of phase separation and surface effects in chromatin compartmentalization, we introduce the mesoscale liquid model of nucleus (MELON), a physical model of nuclear organization that is rooted in the theory of complex fluids. We use diffuse interface finite-element simulations to model the evolution of nuclear chromatin compartments under various developmental processes, including growth and inversion/senescence. Our approach draws inspiration and integrates elements of several mesoscopic cellular models proposed previously. These are the two-fluid fluctuating hydrodynamic model of chromatin (40), deterministic phase-field models of multicellular domain growth (41,42) and its mathematical application to rod chromocenter patterning (43), mesoscale polymeric models of chromatin fiber (20–22), and active cellular mechanics models (44–47). We have applied the MELON framework to model liquid-liquid phase-separation-driven reorganization of the *Drosophila melanogaster* nucleus under different conditions that are characteristic for different cell phases (48,49): interphase, active remodeling phases, long-term senescence, and nuclear inversion (Fig. 1 *A*). Finally, we note that the generic nature of the MELON framework (Fig. 1 *B*), along with the minimal physical assumptions that we have built into the model of the *Drosophila* nucleus, allows drawing broad inferences that should also hold for other eukaryotic nuclei.

MATERIALS AND METHODS

Melon

In this section, we present the basic physics and motivating biology behind MELON. More details about the physical formulation and computational implementation of MELON are in the Supporting Materials and Methods. MELON targets modeling 1) long-timescale chromatin reorganization dynamics, 2) liquid-liquid phase separation of chromatin types, and 3) fluctuations and other nonequilibrium processes of nuclear remodeling. To this end, we have put together a global-free-energy functional based on essential physical features of chromatin: phase separation, surface tension, volume constraints, and specific interaction of chromatin types. The nuclear chromatin morphology is defined through fluctuating order parameters that resolve 1) nuclear membrane $\phi_0(r, t)$; 2) global $i = 1, ..., N$ chromosome territories $\phi_i(r, t)$; and 3) epigenetic states of chromatin $\psi(r, t)$, which smoothly varies from 0 to 1, corresponding to A and B chromatin types, respectively (Fig. 1).

The time evolution of all the order parameters is governed by the global-free-energy functional. The specific forms of the free-energy functional terms are motivated either by basic experimental facts about the chromosomal organization (existence of territories and types) or polymeric physics of chromosomes (excluded volume, demixing of types). The mesoscale

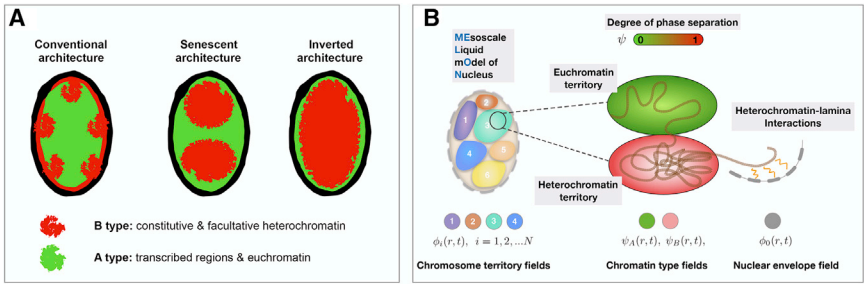

FIGURE 1 (*A*) Schematic representation of commonly observed nuclear architectures for *Drosophila* nucleus including conventional, senescent, and inverted states observed upon loss of lamina-heterochromatin tethering (48,49). (*B*) An illustration of the MELON framework is given. The nucleus is resolved by several marginally overlapping liquid-like chromosomal territories, each of which is described by an individual field variable. Within each chromosomal territory, we introduce an additional variable describing (possible) chromatin phase separation into A or B types that form hetero- or euchromatin droplets. A separate field variable is introduced for describing the elastic membrane and its relaxation dynamics during the events of nuclear growth or inversion. To see this figure in color, go online.

resolution of chromatin naturally accounts for epigenetically driven liquid-liquid phase separation and surface effects of domains, as well as diffusion and fluctuations of liquid chromatin droplets within the nucleus.

After all the relevant interactions are accounted for, the steady-state nuclear morphology is generated by a stochastic search for the global minimum of the free-energy functional in the space of phase-field variables $\boldsymbol{\varphi} = \{\varphi_0, \{\phi_i\}_{i=1,\ldots,N}, \psi\}$:

$$F[\boldsymbol{\varphi}] = F_B[\boldsymbol{\varphi}] + F_R[\boldsymbol{\varphi}] + F_G[\boldsymbol{\varphi}] + F_I[\varphi_0, \psi]. \tag{1}$$

The base-free-energy term F_B accounts for surface energy contribution of chromosomal interfaces and intrachromosomal A-B interfaces. For all domains defined by field variables $\boldsymbol{\varphi} = \{\varphi_0, \{\phi_i\}_{i=1,\ldots,N}, \psi\}$, we assume a simple Landau-Ginzburg form including double-well bulk free-energy and surface contributions:

$$\begin{aligned} F_B[\boldsymbol{\varphi}] = & \int_\Omega d\boldsymbol{\Omega}\left[f_{\text{coex}}(\varphi_0) + \frac{\epsilon_{\varphi_0}^2}{2}(\nabla\varphi_0)^2\right] \\ & + \sum_{i=1}^{N}\int_\Omega d\boldsymbol{\Omega}\left[f_{\text{coex}}(\phi_i) + \frac{\epsilon_{\phi}^2}{2}(\nabla\phi_i)^2\right] \\ & + \int_\Omega d\boldsymbol{\Omega}\left[f_{\text{coex}}(\psi) + \frac{\epsilon_{\psi}^2}{2}(\nabla\psi)^2\right], \end{aligned} \tag{2}$$

where Ω is the domain of the simulation, E coefficients are thickness parameters, and f_{coex} is the free-energy function that maintains coexistence between two chromosomal phases. The restriction term $F_R[\boldsymbol{\varphi}]$ establishes chromosomal territories in the nucleus by penalizing the spatial overlap between chromosomal domains described by field variables ϕ_i.

$$\begin{aligned} F_R[\boldsymbol{\varphi}] = & 4\beta_0 \sum_{i=1}^{N}\int_\Omega d\boldsymbol{\Omega} h(\varphi_0)(1-h(\varphi_0))h(\phi_i) \\ & + \beta_\psi \int_\Omega d\boldsymbol{\Omega}\left[1 - \sum_{i=1}^{N} h(\phi_i)\right]h(\psi) \\ & + \beta_\phi \sum_{i\neq j}^{N}\int_\Omega d\boldsymbol{\Omega} h(\phi_i)h(\phi_j) \end{aligned} \tag{3}$$

The free-energy penalties for excluded volume interactions are introduced via positive volume overlap terms $\beta_{ij}\int_\Omega d\boldsymbol{\Omega} h(\phi_i)h(\phi_j)$ between different domains. The $h(\phi_i)$ functions are standard polynomial forms for approximating volumes of different domains and can be found in the Supporting Materials and Methods. The strength of interaction between different chromatin and nuclear domains are dictated by the energetic prefactors β_{ij}. These prefactors quantify heterochromatin-nuclear envelope soft-excluded volume interactions $\beta\phi_{0\psi} = \beta_0 = const$, chromosome-chromosome soft-excluded volume interactions $\beta_{\varphi_i\varphi_j} = \beta_\varphi = const$, and euchromatin-heterochromatin mixing affinity $\beta_{\psi\varphi_i} = \beta_\psi$ (see Supporting Materials and Methods for numeric values of all the coefficients). The mixing affinity term β_ψ is varied extensively during simulations for investigating the impact of A and B type interactions on nuclear morphology and kinetics of chromatin reorganization during nuclear remodeling processes.

The growth-free-energy term $F_G[\boldsymbol{\varphi}]$ controls the volume growth/shrinking of chromosomal territories upon nuclear volume changes:

$$\begin{aligned} F_G[\boldsymbol{\varphi}] = & \alpha_{Neq}\left[\overline{V}_N - V_N(t)\right]^2 + \alpha_N\left[V_N(t) - \sum_{i=1}^{N} V_i(t)\right]^2 \\ & + +\alpha_V \sum_{i=1}^{N}\left[V_i(t) - \overline{V}_i(t)\right]^2 + \alpha_v \sum_{i=1}^{N}\left[v_i(t) - \overline{v}_i(t)\right]^2. \end{aligned} \tag{4}$$

The growth terms are defined via the harmonic restraint $\alpha_i(V_i - \overline{V}_i)^2$ terms that favor stable domain size for the nucleus V_N, chromosomal territories $\overline{V}_i$, and heterochromal territories $\overline{v}_i$. The energetic prefactors α_i govern the strength of domain localization (see Supporting Materials and Methods for more information). A similar formulation of domain growth terms as volume constraints in free energy has been used by Nonomura in applications of phase-field methods to multicellular growth models (41) and recently also by Lee et al. (43) for mathematical modeling of chromocenter patterns of rods. Recent experiments and simulations have shown that nuclear chromatin organization is highly correlated with the integrity of the chromatin-lamina scaffold (48,50), which regulates chromatin dynamics during development. To highlight the effect of nuclear shape dynamics on chromatin reorganization, it is important to couple the nuclear shape dynamics with chromatin state variables. The $F_I[\phi_0, \psi]$ term accounts for heterochromatin-lamina interactions giving rise to the so-called lamina-associating domains formed by heterochromatin regions (51). Lamina-associating domains have a significant nuclear presence and are localized near the inner nuclear membranes in most of the mammalian nuclei.

We model this aspect of nuclear architecture by a strong membrane affinity term that keeps heterochromatin preferentially clustered in the vicinity of the membrane region. This preferential interaction of heterochromatin with nuclear lamina is realized via interfacial free-energy functional:

$$F_I[\varphi_0, \psi] = \gamma\int_\Omega d\boldsymbol{\Omega}\nabla h(\varphi_0)\cdot\nabla h(\psi), \tag{5}$$

where γ is a binding affinity coefficient quantifying how strong heterochromatin is "attracted to" nuclear lamina or nuclear envelope relative to intrachromosomal interactions. After specifying the full free-energy functional of the nucleus (Eqs. 1, 2, 3, 4, and 5), the dynamic equations can be written for each phase-field variable using an Allen-Cahn prescription (52):

$$\frac{\partial \varphi_0}{\partial t} = -L_{\varphi_0}\frac{\delta F}{\delta \varphi_0}; \qquad \frac{\partial \phi_i}{\partial t} = -L_{\phi_i}\frac{\delta F}{\delta \phi_i}\bigg|_{(i=1,\ldots,N)};$$
$$\frac{\partial \psi}{\partial t} = -L_{\psi}\frac{\delta F}{\delta \psi} + \eta_{\psi}(\mathbf{r},t). \tag{6}$$

The term η_ψ accounts for fluctuations at the boundaries of euchromatin and heterochromatin islands due to the finite size nature of droplets. The fluctuations are modeled as Brownian noise: $\langle \eta_\psi(\mathbf{r},\ t)\eta_\psi(\mathbf{r}',\ t')\rangle = A_p\delta(\mathbf{r}-\mathbf{r}')\delta(t-t')$, where the amplitude of noise $A_p = 2k_BT_{eff}L_\psi$ sets the "effective temperature" T_{eff} of the nucleus (40), which can be taken as a measure of ATP activity in comparisons with experiment (53,54). We note that in the MELON framework, one can readily introduce active processes and driven fluctuations in chromatin liquid droplets (53,54). The timescale of chromatin relaxation is set by $\tau = L^{-1}$. It is well-known that in different developmental stages of eukaryotic cells, the dynamics of nuclear processes proceed on vastly different timescales. Therefore, when modeling nuclear rearrangements in postembryonic interphase, we set $\tau = 5 \times 10^{-3}$ h, and when modeling long-term nuclear senescence, we set $\tau = 5$ h to match the relevant timescales of attaining different nuclear morphology.

MELON: A physical simulator of liquid-liquid phase transitions in the nucleus

Here, we place the MELON framework in the context of previous efforts in applying continuum diffuse interface methods for modeling cellular phenomena. The two-fluid model of chromatin proposed by Bruinsma et al. (40) was the first work to suggest the broad usefulness of field-theoretic models for incorporating thermal fluctuations, active processes, and chromatin hydrodynamics under one framework. In recent years, field theoretical methods and the phase-field methods in particular have emerged as powerful techniques for modeling cellular phenomena from protein coacervation (55) to membrane deformation (56–58) and cell division (41,42). An important class of models originally developed for modeling multicellular growth based on the phase-field approach have introduced important numerical techniques for modeling domain growth processes under volume constraints. The domain-growth free-energy functional pioneered by Nonomura et al. (41,42) in particular has inspired many applications. This functional takes into account different forces such as cell adhesion, volume constraints, and excluded volume interaction. A mathematical application of multicellular growth model (41) to single-cell objects was presented in the work of Lee et al. (43), in which the free-energy functional of Nonomura (41) was used for generating chromocenter patterns of rod cells and studying patterns with respect to domain volume adjustment. In this model, the cell shape and size nucleus variation are treated via a mathematical translation operation that is uncoupled to any of the internal field variables. Furthermore, mathematical switching functions of phase variables have been utilized to change field variables halfway through pattern rod chromocenter generation. This approach comes with a cost of operating a large number of auxiliary parameters that are manually adjusted for generating each target pattern.

The objective for developing MELON is to have a stochastic physical simulator that models passive fluctuations, liquid-liquid phase separation, and lamina-anchoring closely mimicking soft polymeric nature of chromatin. Compared to mathematical and deterministic applications of diffuse interphase or related continuum models, there are very few parameters, most of which are fixed and mirror coarse-grained polymeric objects in the nucleus. This is achieved by modifying the standard domain-growth free-energy functional such as found in Nonomura et al., namely 1) membrane envelope is explicitly resolved with a new variable, and dynamics is propagated by coupling to constant timescale viscous relaxation; 2) new coupling terms between chromosomal domains of the nucleus have been introduced. This latter couples all the fields together and with membrane, thereby acting as dense polymeric material; and 3) thermal noise that couples A and B type fluctuations in heterochromatin and euchromatin territories.

The MELON framework has been coded in C++ using the finite-element numerical library MOOSE (59,60). Nuclear morphology visualizations have been generated via Python-based Paraview (61).

RESULTS

Impact of chromosome territorial affinity and heterochromatin-lamina interactions on euchromatin and heterochromatin phase separation

To illustrate the consequences of liquid behavior and phase separation of A and B chromatin types in the nucleus, we apply MELON to model the *Drosophila* nucleus in its various developmental stages (Fig. 1 *A*). Recent experiments suggest that liquid-liquid phase separation of chromatin domains in *D. melanogaster* nuclei is orchestrated by HP1a proteins, which, under favorable conditions, would form liquid condensates and dissolve heterochromatin regions within liquid droplets (31,32,62). Polymer models have shown the importance of A and B phase separation (16,17) as one of the main driving forces behind chromatin organization in mammals. Heterochromatin-lamina interactions (50,63,64) are instead thought to be responsible for the switching between conventional and inverted nuclear morphology.

Using our diffuse interface model of the nucleus, we investigate the role of various terms in the global-free-energy functional in generating steady-state nuclear morphology liquid-liquid phase-separation dynamics. We set the average heterochromatin content of the nucleus at 25%, corresponding to the postembryonic stage of the *Drosophila* nucleus (65). Later on, we will vary this content when investigating the impact of heterochromatin content on the dynamics of phase separation and the resulting nuclear morphology.

To describe chromatin dynamics in the nucleus quantitatively, we evaluate the temporal evolution of the summed volumes of individual chromosomes $V(t)$ and heterochromatin droplets from all chromosomes $v(t)$. The simulations that generate starting nuclear morphologies (Fig. 2 *A*; Videos S1 and S2) show that volumes $V(t)$ and $v(t)$ evolve until the nucleus is filled with liquid state chromatin, at which point a steady state is reached in which compartments acquire well-defined volumes. After coexistence between different liquid chromatin compartments is reached, we investigate how variations of interaction strengths defined

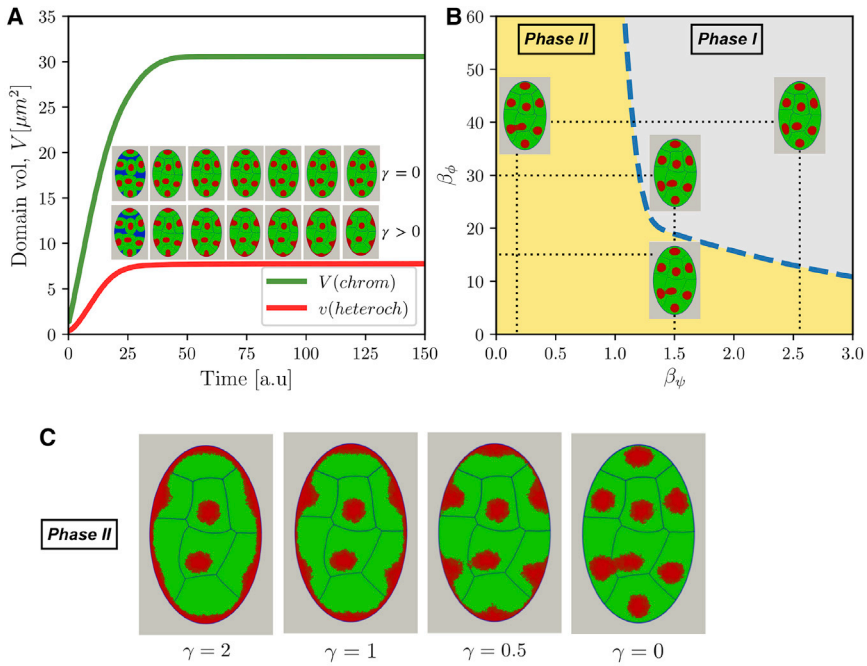

FIGURE 2 (*A*) Evolution of chromosomal and heterochromatin volume in the idealized nucleus with and without heterochromatin-lamina interactions ($\gamma > 0$ and $\gamma = 0$). The snapshots show the nuclear morphology at different times (every 24 time steps) during the generation stage of the nucleus with and without heterochromatin-lamina interactions. The nuclear compartment is colored in blue, chromosome territory in green, and heterochromatin compartment in red. (*B*) A phase diagram of nuclear morphology showing the impact of various constraints and affinities on liquid-liquid phase separation of A and B domains in the formation of heterochromatin and euchromatin territories is given. Phases are defined in terms of connectivity between heterochromatin droplets (continuous versus discontinuous or piecewise continuous variation of ψ variable; see also Supporting Materials and Methods). Phase I corresponds to a fully disconnected and mixed state; phase II corresponds to strongly connected and demixed or partially demixed states. (*C*) The impact of lamina-heterochromatin anchoring affinity variation on the emergent nuclear morphology is shown. To see this figure in color, go online.

in the previous section alter the coexistence state of the nucleus.

We first investigate the impact of chromosome-type-mixing affinity β_ϕ and β_ψ, of which the latter governs the interaction range between chromatin compartments. We see that for a given chromosomal interaction range β_ϕ, a strong affinity leads to mixed states for heterochromatin droplets, whereas weaker mixing affinity leads to fusion of heterochromatin droplets (Fig. 2 *B*).

Variation of nuclear membrane lamina-heterochromatin interaction shows that nuclear morphology is significantly affected by the changes in lamina-anchoring strength (Fig. 2 *C*). This is unsurprising given the large surface area of the nuclear envelope. Indeed, when we set a nonzero affinity $\gamma > 0$ for the lamina interactions, the heterochromatin shows pronounced localization near the nuclear envelope. In the presence of dominant lamina-heterochromatin interactions, the impact of mixing affinity is now seen in different thicknesses of the heterochromatin belt formed around the nuclear envelope. This somewhat subtle difference is due to the competition between the lamina binding energy (negative term in the global $F[\phi]$) and territorial interaction energy (positive term in the global $F[\phi]$). Thus, consistent with optical microscopy observations (65,66) and polymer simulations (50,63), the lamina binding affinity is indeed one of the dominant physical interactions that shape conventional nuclear architecture.

Loss of affinity has been shown to lead to an inversion of nuclear architecture, which we show is a naturally emerging behavior of our model of the nucleus (66,67). In the subsequent sections, we show that the inversion behavior, along with its characteristic kinetics, is naturally explained by liquid-like behavior of chromatin.

Impact of diffusion, fluctuations, and heterochromatin content on formation of liquid chromatin compartments

In this section, we study the roles of heterochromatin droplet diffusion, fluctuations, and nuclear heterochromatin fraction on the kinetics of phase separation in the idealized nucleus during interphase and senescent phases. The setup of the first set of simulation is mimicking the rapid liquid-like nucleoprotein droplet fusion events during interphase, the dynamics of which have been observed and quantified in multiple recent experiments (31,32,68). It is acknowledged that within an in vivo nucleoplasm environment, heterochromatin droplets display shape and size fluctuations as a result of thermal fluctuations and active, ATP-driven motor activity (69). In this scheme of the MELON framework, we model fluctuations by a thermal noise term that accounts for the fluctuations of finite-sized droplets in an effective manner. Introduction of fluctuation term, however, has allowed us to quantify how "effective temperature" in the nucleus impacts the kinetics of phase separation. To this end, we have carried out simulations with fixed nuclear volume while varying fluctuation amplitude values.

We find that passive fluctuations lead to enhancement of liquid droplet contact and fusion events, which in turn enhance the kinetics of phase separation in the nucleus (Fig. 3, *A* and *B*). To be more quantitative, we have evaluated the droplet fusion time τ_c for different fluctuation

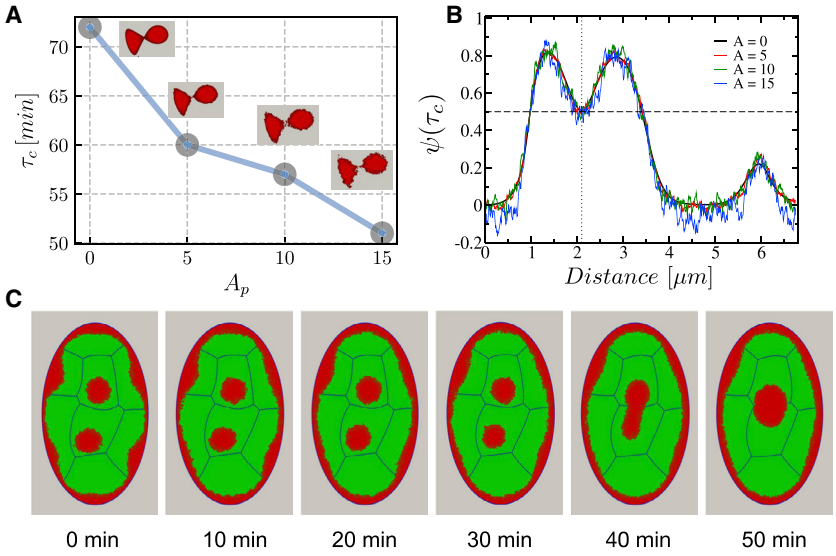

FIGURE 3 Impact of euchromatin and heterochromatin boundary fluctuations on the heterochromatin droplet fusion dynamics. Shown are (*A*) the profile of droplet fusion time τ_c as a function of droplet fluctuation amplitude A_p; (*B*) the fluctuation profile along the heterochromatin order parameter; and (*C*) representative snapshots of droplet fusion dynamics for $A_p = 10$ amplitude and postembryonic interphase cycle, for which chromatin relaxation timescale is set as $\tau = L^{-1} = 5 \times 10^{-3}$ h. To see this figure in color, go online.

amplitudes A_p (Fig. 3 *A*). Thus, the fluctuation amplitude of heterochromatin-euchromatin interfaces effectively increases the capture radius or diffusion coefficient of the liquid droplets (Fig. 3, *A* and *B*). Finally, the comparison with experiments probing in vivo nucleoplasm (68) shows that the liquid state model of chromatin in the MELON framework accurately captures the nuclear coalescence profiles, as well as surface profiles and sequence of steps on time-lapse nuclear domain coalescence events (Fig. 3, *B* and *C*).

Next, we fix the fluctuation amplitude of droplets at a fixed moderate value and examine a process of large-scale nuclear reorganization that is initiated by severing the lamina and heterochromatin. These types of simulations serve as a point of comparison with nuclear volume remodeling simulations of senescence and inversion reported in the next section. Starting from a conventional nuclear morphology with 25% of heterochromatin fraction content, we monitor droplet fusion leading to partial phase separation of heterochromatin. Consistent with the microscopy experiments (65–67), the conventional morphology of the nucleus, in response to the disruption of heterochromatin-lamina anchoring, evolves toward a morphology with fewer heterochromatic centers, which are localized in the center of the nucleus (Fig. 4 *A*). During the reorganization stage, the adjacent heterochromatin droplets fuse, thereby reducing

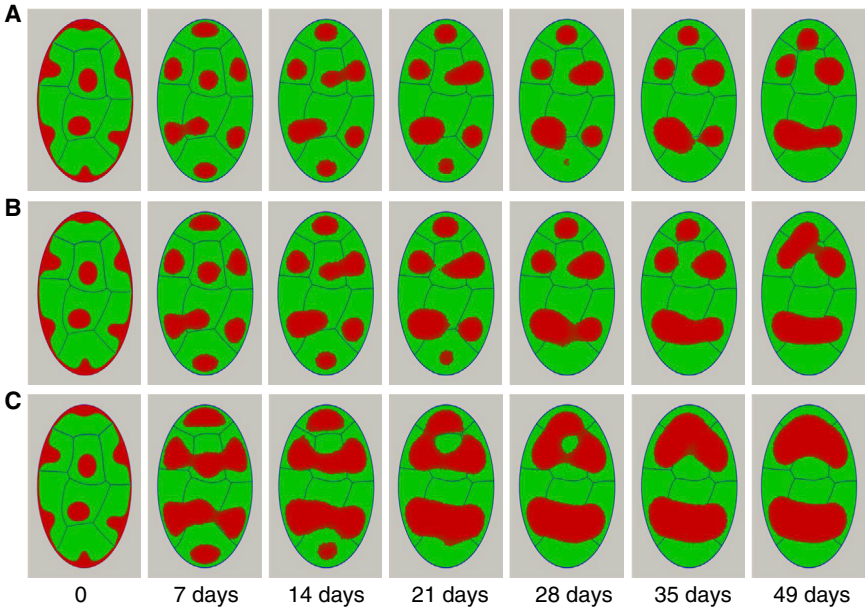

FIGURE 4 Impact of heterochromatin volume fraction on the nuclear compartment reorganization with fixed nuclear size. Shown are nuclear morphologies generated with different heterochromatin contents: (*A*) $\rho = 25\%$, (*B*) $\rho = 30\%$, and (*C*) $\rho = 45\%$. Simulations are initiated by terminating lamina-heterochromatin interaction, and the timescale of chromatin relaxation is set for modeling nuclear senescence and inversion $\tau = L^{-1} = 5$ h. $A_p = 5$ for mammalian nuclei (65). To see this figure in color, go online.

the number of chromocenters in the nucleus (Fig. 4 *A*). To predict the impact of heterochromatin mobility and its fraction in the nucleus on phase-separation kinetics, we performed simulations with different values of heterochromatin fractions and different diffusion coefficients. To do this, we assume that during the nuclear reorganization, the heterochromatin continues growing to reach the prescribed fraction. Indeed, changing the heterochromatin fraction in conventional nuclear architecture to a newly prescribed fraction in inverted architecture should not impact the displacement and fusion of heterochromatin droplets strongly because the growth kinetics of heterochromatin is very fast relative to heterochromatin mobility. Fig. 4, *B* and *C* represent the inverted nuclear architecture obtained for 30 and 45% of heterochromatin fraction content in the nucleus. As one would expect, the higher heterochromatin content leads to faster phase separation associated with a decrease in the clustered heterochromatin number.

The displacement of the heterochromatin droplets within the nucleus is controlled by the diffusion coefficient which is related to the thickness of euchromatin-heterochromatin interfacial region. The simulation results performed for a given heterochromatin fraction (30%) and a fixed nuclear volume showed that increasing the diffusion coefficient accelerates the fusion of heterochromatin droplets to form two clusters at the steady state of nuclear morphology for a higher value (Fig. S3). Additionally, we find there to be a critical threshold, the exceeding of which leads to a fully phase-separated morphology given reasonable diffusion constants and absence of any desegregating lamina-heterochromatin interactions.

Interplay between chromatin phase separation and nuclear volume remodeling accompanying senescence

The cell nucleus is subject to continuous remodeling activity changing volume, shape, or internal organization in response to a variety of external or internal signals. For instance, during the interphase, eukaryotic nuclei undergo steady expansion until mitosis (70). During senescence (71) and embryonic development (65,66), however, the nucleus can lose lamina-heterochromatin affinity and undergo large-scale redistribution of chromatin in which heterochromatin moves away from the periphery to a region closer to the center of the nucleus (Fig. 1). These large-scale chromatin remodeling events are often accompanied by expanding and shrinking of nuclear volume (66). Given the frequency with which nuclear volume/shape change and chromatin reorganization happen together, one may expect there to be robust mechanisms tuned with volume drift and fluctuations.

Phase separation of chromatin domains provides one such robust mechanism for rapid mobilization of a large section of the genome with predictable dependence on volume changes. In this context, it is therefore worthwhile to investigate in detail how the kinetics of chromatin phase separation is coupled with the remodeling of nuclear volume.

To this end, we have carried out simulations that mimic processes of nuclear senescence and inversion happening on the timescale of days and resulting in a dramatic change in nuclear volume and euchromatin/heterochromatin.

Within our MELON framework, remodeling of the nuclear volume is simulated by uniaxial slow compression/expansion of membrane boundaries, which allows the liquid chromatin compartments to expand/contract. The volume remodeling processes considered are all propagated at a constant rate, which is taken to be much slower than any of the intranuclear diffusion timescales: $\tau_{remod} = L_{\varphi_0}^{-1} \ll \tau_{A/B} = L_{\psi}^{-1}$. In this work, we did not consider anisotropic deformations and fluctuations of the nuclear envelope (69), which certainly could be an interesting question that merits separate investigation.

Fig. 5 shows the impact of nuclear volume changes on chromatin reorganization dynamics in the absence of heterochromatin-lamina interactions. We see that in all cases, heterochromatin and euchromatin distribution is driven toward completely phase-separated states, with heterochromatin accumulating in the vicinity of the nuclear core. However, the kinetics and morphology of this transition are markedly different relative to constant volume case of the previous section. This shows that chromatin diffusion rates and volume remodeling rates can be in a tug of war with each other. Additionally, we see that the chromosome territories can remain well-separated during the remodeling of nuclear volume, which suggests that coexistence of key subnuclear compartmentalization of A and B types with optimal affinity can be made robust to volume remodeling.

To quantify the dynamics of heterochromatin and euchromatin phase separation, we have investigated how the number of heterochromatin clusters varies with target nuclear volume while keeping remodeling times fixed. The results show that the value of final volume leads to more rapid phase separation because, in smaller nuclear volumes, the encounter rates of heterochromatin droplets are higher (Fig. 6). Indeed, the distance between the two regions occupied by heterochromatin becomes small when the nuclear volume decreases; hence, the fusion between them becomes more favorable. Because the relaxation time of the nuclear envelope $(L_{\varphi_0} = const)$ is being kept constant, it is also interesting to evaluate the characteristic time of relaxation of heterochromatin domains to assess how much the dynamics of internal chromatin motions are affected. We find that the chromosome territories relaxed to their equilibrium volume with a nearly same relaxation time of the nucleus, whereas the heterochromatin domains relaxed faster (Fig. 6; Table S1).

Likewise, the diffusion rates and rate of volume reduction lead to a nearly uniform acceleration of the dynamics of droplet fusion events. We see that nuclear growth works

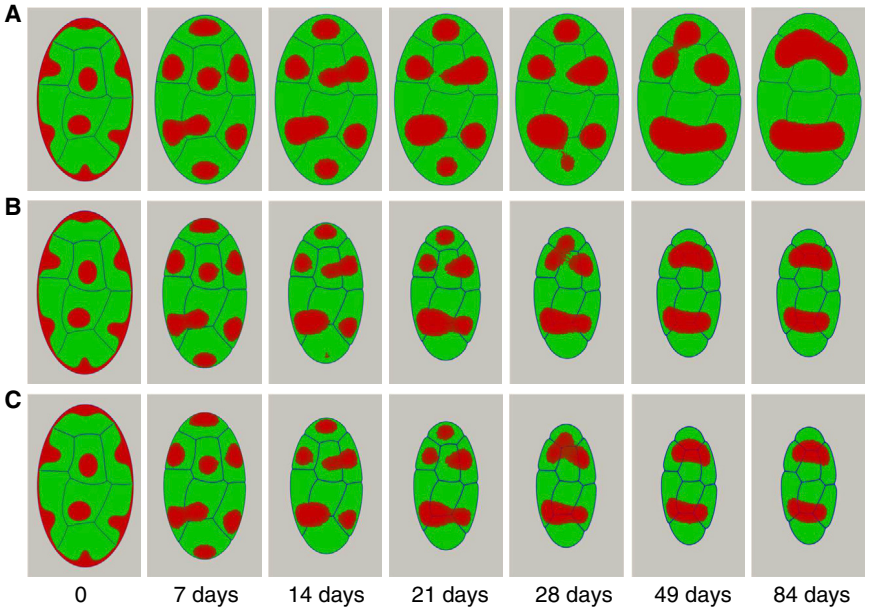

FIGURE 5 Impact of nuclear volume remodeling on euchromatin and heterochromatin phase separation. Shown are simulations that remodel nuclear volume by (*A*) nuclear growth with 10% volume expansion, (*B*) uniform nuclear compression of oblate nuclear envelope by 50%, and (*C*) nuclear compression by 60%. Overall heterochromatin fraction content in the nucleus is fixed at 30%. To see this figure in color, go online.

against phase separation and, in principle, can slow it down or arrest it for some parameter regimes. Based on experimental observations (67), the time required for the complete transformation of the conventional architecture of mammalian nuclei to inverted morphology is predicted to take on the order of ∼30 days, with the corresponding heterochromatin cluster number estimated to be 2–3. The results with the embryonic timescale adopted in this work thus agree quantitatively with the experiments (67).

In the case of nuclear inversion, we find that the thermodynamic driving force of phase separation ensures robust evolution of chromatin toward steady-state nuclear morphologies with respect of heterochromatin content, final volume, and diffusion rate variations (Figs. S4–S6). This robustness is a generic feature of phase separations and has been remarked in many related prior studies using phase-field methods such as the ones by Nonomura (41) in the context of multicellular growth and Lee et al. (43) in the context of rod chromocenters.

Finally, we have explored the conditions under which heterochromatin domains merge into a single cluster, which is commonly seen in rod cells upon complete nuclear inversion (Fig. 7). Scanning the phase space of nuclear morphology along the heterochromatin density axis (see Supporting Materials and Methods), we have found that the specific condition favoring single cluster formation is having at least 50% heterochromatin content, which, in the MELON framework, would correspond to combined constitutive and facultative heterochromatin content.

The observations of nuclear inversion have recently attracted considerable attention in studies employing computer simulations and applied mathematics. In particular, we mention here the important work of Falk et al. (64),

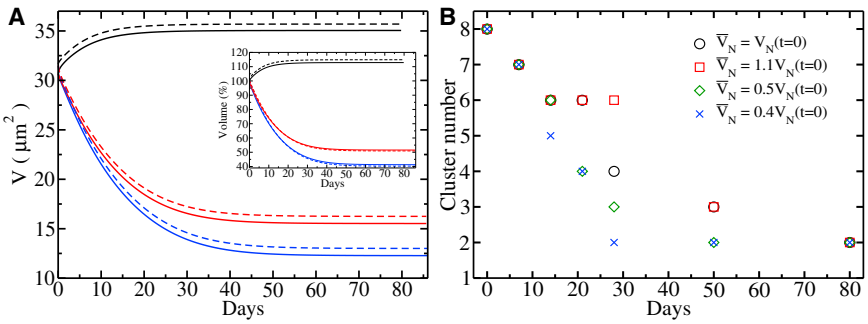

FIGURE 6 (*A*) Volume relaxation profiles of chromosomes (*solid lines*) and nucleus as a whole (*dashed lines*) as a function of remodeling time. The color code shows the different target of steady-state nuclear volumes corresponding to 10% volume expansion (*black lines*), volume compression by 50% (*red lines*), and volume compression by 60% (*blue lines*). (*B*) Temporal evolution of the number of heterochromatin cluster in the cell's nucleus during the reorganization process with different target steady-state nuclear volumes $\overline{V}_N$ is shown. All simulations of the nuclear volume remodeling were initiated by terminating heterochromatin-lamina interaction term to mimic processes of senescence and nuclear inversion. The heterochromatin fraction content in the nucleus is fixed to 30%. To see this figure in color, go online.

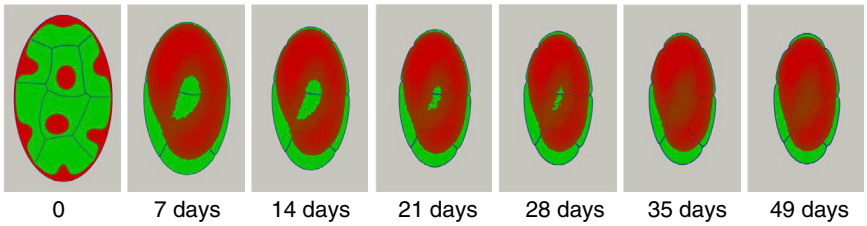

FIGURE 7 An example of single heterochromatic cluster formation. Heterochromatin fraction in the nucleus is elevated to 60% to account for the existence of high combined facultative and constitutive heterochromatin. We have used ~10 times higher diffusion coefficient (relative to simulations in Figs. 2, 3, 4, 5, and 6) to accelerate phase separation. To see this figure in color, go online.

who have used an A-B-C heteropolymeric model of chromatin to identify the balance of type interaction that leads to inverted architecture. In another work by Lee et al. (43), a mathematical application of phase-field methodology based on Nonomura's multicellular growth model (41) was employed to generate inverted nuclear patterns of single rod cells. As opposed to this work and work by Falk et al. (64), however, the inversion was realized via a purely mathematical deterministic protocol of using ad hoc transnational operators acting on cell envelope and sigmoidal functions adjusting chromatin fractions halfway during protocols. Within the framework of MELON, the nuclear inversion emerges organically as a result of noise-driven dynamical relaxation of chromatin domains upon severing lamina-heterochromatin anchoring. Furthermore, our simulations indicate the existence of a critical fraction of heterochromatin without which full inversion is hampered.

CONCLUSIONS

In recent years, there has been a gradual shift away from the paradigm of static regular fiber organization of chromatin to a paradigm of fluid-like, heterogeneous, and dynamic order. This paradigm shift has been further catalyzed by the latest series of experiments, which have implicated disordered proteins with known nuclear regulatory functions for driving the liquid-liquid phase separation of chromatin regions in the nucleus (31,32,72,73). Additionally, several theoretical models (74–77) and computer simulations of chromatin polymer (17,34,64,78) have shown the broad consistency of the heterogeneous copolymer melt view of chromatin with the Hi-C and single-molecule data.

Thus, a natural question that emerges from these observations is how much of large-scale chromatin ordering and dynamics in the nucleus could be explained away just by the fluid-like behavior of chromatin? This question is especially pressing if one wants to create viable models of long-time-scale development of eukaryotic nuclei such as in aging, differentiation, and disease propagation.

To begin answering these questions, we have constructed MELON, a streamlined computational framework in which chromatin is resolved as a fluctuating fluid mixture composed of epigenetically colored components. Using this model, we find that a fluid description of chromatin combined with basic facts about the nuclear architecture, including the existence of chromosomal territories, A and B epigenetic type interactions, and lamina-heterochromatin anchoring, leads to life-like nuclear morphologies. Application of the MELON framework to the *Drosophila* nucleus at different developmental stages of the nucleus such as interphase, long-time senescence, and inversion reveals a rich interplay between liquid-liquid phase separation, nucleation, and droplet fluctuations. We would like to emphasize further that the generic nature of the model and the minimal assumptions that we have built into it allow one to draw conclusions that should generally be applicable for a wide variety of eukaryotic nuclei and not just for the *Drosophila* nucleus. Particularly, our study finds that a significant role is played by surface tension and lamina-heterochromatin interactions in determining large-scale chromatin rearrangements. Our study introduces an innovative approach for studying micron-scale chromatin dynamics; we foresee that further development of the method here introduced—the MELON framework—will shed new light on the microrheology, the diffusive behavior, and the hydrodynamics of nuclear chromatin.

SUPPORTING MATERIAL

Supporting Material can be found online at https://doi.org/10.1016/j.bpj.2019.09.013.

AUTHOR CONTRIBUTIONS

R.L. and D.A.P. designed the research. R.L. carried out all simulations. R.L. and D.A.P. analyzed the data. R.L., M.D.P., and D.A.P. did the literature review and conceptualization. R.L., M.D.P., and D.A.P. wrote the article.

ACKNOWLEDGMENTS

D.A.P. and R.L. acknowledge useful discussions with Xueyu Song and Jim Evans.

D.A.P. is grateful for the financial support from the Caldwell Foundation of Iowa State. M.D.P.'s research is supported by the Center for Theoretical Biological Physics sponsored by the National Science Foundation (grants PHY-1427654 and NSF-CHE-1614101) and by the Welch Foundation (Grant C-1792). All the simulations in the manuscript were carried out using the National Science Foundation's XSEDE allocation on Stampede2 machine at the service provider through allocations MCB180058 and MCB180071.

REFERENCES

1. Alberts, B. 2015. Molecular Biology of the Cell. Garland Science, Taylor and Francis Group, New York.
2. Phillips, R. 2013. Physical Biology of the Cell. Garland Science, London.
3. Lieberman-Aiden, E., N. L. van Berkum, …, J. Dekker. 2009. Comprehensive mapping of long-range interactions reveals folding principles of the human genome. *Science.* 326:289–293.
4. Dixon, J. R., I. Jung, …, B. Ren. 2015. Chromatin architecture reorganization during stem cell differentiation. *Nature.* 518:331–336.
5. Chathoth, K. T., and N. R. Zabet. 2019. Chromatin architecture reorganization during neuronal cell differentiation in *Drosophila* genome. *Genome Res.* 29:613–625.
6. Bonev, B., N. Mendelson Cohen, …, G. Cavalli. 2017. Multiscale 3D genome rewiring during mouse neural development. *Cell.* 171:557–572.e24.
7. Lin, Y. T., P. G. Hufton, …, D. A. Potoyan. 2018. A stochastic and dynamical view of pluripotency in mouse embryonic stem cells. *PLoS Comput. Biol.* 14:e1006000.
8. Folguera-Blasco, N., R. Pérez-Carrasco, …, T. Alarcón. 2019. A multiscale model of epigenetic heterogeneity-driven cell fate decision-making. *PLoS Comput. Biol.* 15:e1006592.
9. Meldi, L., and J. H. Brickner. 2011. Compartmentalization of the nucleus. *Trends Cell Biol.* 21:701–708.
10. Rao, S. S., M. H. Huntley, …, E. L. Aiden. 2014. A 3D map of the human genome at kilobase resolution reveals principles of chromatin looping. *Cell.* 159:1665–1680.
11. Heitz, E. 1928. Das Heterochromatin der Moose. *Jahrb. Wiss. Bot.* 69:762–818.
12. Imai, R., T. Nozaki, …, K. Maeshima. 2017. Density imaging of heterochromatin in live cells using orientation-independent-DIC microscopy. *Mol. Biol. Cell.* 28:3349–3359.
13. Grimm, J. B., B. P. English, …, L. D. Lavis. 2015. A general method to improve fluorophores for live-cell and single-molecule microscopy. *Nat. Methods.* 12:244–250, 3 p following 250.
14. Ou, H. D., S. Phan, …, C. C. O'Shea. 2017. ChromEMT: visualizing 3D chromatin structure and compaction in interphase and mitotic cells. *Science.* 357:eaag0025.
15. Di Pierro, M., B. Zhang, …, J. N. Onuchic. 2016. Transferable model for chromosome architecture. *Proc. Natl. Acad. Sci. USA.* 113:12168–12173.
16. Di Pierro, M., R. R. Cheng, …, J. N. Onuchic. 2017. De novo prediction of human chromosome structures: epigenetic marking patterns encode genome architecture. *Proc. Natl. Acad. Sci. USA.* 114:12126–12131.
17. Di Pierro, M., D. A. Potoyan, …, J. N. Onuchic. 2018. Anomalous diffusion, spatial coherence, and viscoelasticity from the energy landscape of human chromosomes. *Proc. Natl. Acad. Sci. USA.* 115:7753–7758.
18. Barbieri, M., M. Chotalia, …, M. Nicodemi. 2012. Complexity of chromatin folding is captured by the strings and binders switch model. *Proc. Natl. Acad. Sci. USA.* 109:16173–16178.
19. Jost, D., P. Carrivain, …, C. Vaillant. 2014. Modeling epigenome folding: formation and dynamics of topologically associated chromatin domains. *Nucleic Acids Res.* 42:9553–9561.
20. Bascom, G. D., C. G. Myers, and T. Schlick. 2019. Mesoscale modeling reveals formation of an epigenetically driven HOXC gene hub. *Proc. Natl. Acad. Sci. USA.* 116:4955–4962.
21. Bascom, G. D., and T. Schlick. 2018. Mesoscale modeling of chromatin fibers. *In* Nuclear Architecture and Dynamics. Elsevier, pp. 123–147.
22. Di Pierro, M. 2019. Inner workings of gene folding. *Proc. Natl. Acad. Sci. USA.* 116:4774–4775.
23. MacPherson, Q., B. Beltran, and A. J. Spakowitz. 2018. Bottom-up modeling of chromatin segregation due to epigenetic modifications. *Proc. Natl. Acad. Sci. USA.* 115:12739–12744.
24. Li, P., S. Banjade, …, M. K. Rosen. 2012. Phase transitions in the assembly of multivalent signalling proteins. *Nature.* 483:336–340.
25. Brangwynne, C. P., C. R. Eckmann, …, A. A. Hyman. 2009. Germline P granules are liquid droplets that localize by controlled dissolution/condensation. *Science.* 324:1729–1732.
26. Banjade, S., and M. K. Rosen. 2014. Phase transitions of multivalent proteins can promote clustering of membrane receptors. *eLife.* 3:e04123.
27. Brangwynne, C. P., T. J. Mitchison, and A. A. Hyman. 2011. Active liquid-like behavior of nucleoli determines their size and shape in *Xenopus laevis* oocytes. *Proc. Natl. Acad. Sci. USA.* 108:4334–4339.
28. Brangwynne, C. P., P. Tompa, and R. V. Pappu. 2015. Polymer physics of intracellular phase transitions. *Nat. Phys.* 11:899–904.
29. Uversky, V. N. 2017. Protein intrinsic disorder-based liquid-liquid phase transitions in biological systems: complex coacervates and membrane-less organelles. *Adv. Colloid Interface Sci.* 239:97–114.
30. Boeynaems, S., S. Alberti, …, M. Fuxreiter. 2018. Protein phase separation: a new phase in cell biology. *Trends Cell Biol.* 28:420–435.
31. Strom, A. R., A. V. Emelyanov, …, G. H. Karpen. 2017. Phase separation drives heterochromatin domain formation. *Nature.* 547:241–245.
32. Larson, A. G., D. Elnatan, …, G. J. Narlikar. 2017. Liquid droplet formation by HP1α suggests a role for phase separation in heterochromatin. *Nature.* 547:236–240.
33. Shin, Y., and C. P. Brangwynne. 2017. Liquid phase condensation in cell physiology and disease. *Science.* 357:eaaf4382.
34. Liu, L., G. Shi, …, C. Hyeon. 2018. Chain organization of human interphase chromosome determines the spatiotemporal dynamics of chromatin loci. *PLoS Comput. Biol.* 14:e1006617.
35. Nuebler, J., G. Fudenberg, …, L. A. Mirny. 2018. Chromatin organization by an interplay of loop extrusion and compartmental segregation. *Proc. Natl. Acad. Sci. USA.* 115:E6697–E6706.
36. Sanborn, A. L., S. S. Rao, …, E. L. Aiden. 2015. Chromatin extrusion explains key features of loop and domain formation in wild-type and engineered genomes. *Proc. Natl. Acad. Sci. USA.* 112:E6456–E6465.
37. Bronshtein, I., E. Kepten, …, Y. Garini. 2015. Loss of lamin A function increases chromatin dynamics in the nuclear interior. *Nat. Commun.* 6:8044.
38. Lucas, J. S., Y. Zhang, …, C. Murre. 2014. 3D trajectories adopted by coding and regulatory DNA elements: first-passage times for genomic interactions. *Cell.* 158:339–352.
39. Zidovska, A., D. A. Weitz, and T. J. Mitchison. 2013. Micron-scale coherence in interphase chromatin dynamics. *Proc. Natl. Acad. Sci. USA.* 110:15555–15560.
40. Bruinsma, R., A. Y. Grosberg, …, A. Zidovska. 2014. Chromatin hydrodynamics. *Biophys. J.* 106:1871–1881.
41. Nonomura, M. 2012. Study on multicellular systems using a phase field model. *PLoS One.* 7:e33501.
42. Akiyama, M., M. Nonomura, …, R. Kobayashi. 2018. Numerical study on spindle positioning using phase field method. *Phys. Biol.* 16:016005.
43. Lee, S. S., S. Tashiro, …, R. Kobayashi. 2017. A new application of the phase-field method for understanding the mechanisms of nuclear architecture reorganization. *J. Math. Biol.* 74:333–354.
44. Ghaffarizadeh, A., R. Heiland, …, P. Macklin. 2018. PhysiCell: an open source physics-based cell simulator for 3-D multicellular systems. *PLoS Comput. Biol.* 14:e1005991.
45. Deviri, D., D. E. Discher, and S. A. Safran. 2017. Rupture dynamics and chromatin herniation in deformed nuclei. *Biophys. J.* 113:1060–1071.
46. Sen, S., A. J. Engler, and D. E. Discher. 2009. Matrix strains induced by cells: computing how far cells can feel. *Cell. Mol. Bioeng.* 2:39–48.

47. Knežević, M., H. Jiang, and S. Wang. 2018. Active tuning of synaptic patterns enhances immune discrimination. *Phys. Rev. Lett.* 121:238101.

48. Ulianov, S. V., S. A. Doronin, …, Y. Y. Shevelyov. 2019. Nuclear lamina integrity is required for proper spatial organization of chromatin in Drosophila. *Nat. Commun.* 10:1176.

49. Jagannathan, M., R. Cummings, and Y. M. Yamashita. 2019. The modular mechanism of chromocenter formation in *Drosophila*. *eLife*. 8:e43938.

50. Kinney, N. A., I. V. Sharakhov, and A. V. Onufriev. 2018. Chromosome-nuclear envelope attachments affect interphase chromosome territories and entanglement. *Epigenetics Chromatin.* 11:3.

51. van Steensel, B., and A. S. Belmont. 2017. Lamina-associated domains: links with chromosome architecture, heterochromatin, and gene repression. *Cell.* 169:780–791.

52. Allen, S. M., and J. W. Cahn. 1979. A microscopic theory for antiphase boundary motion and its application to antiphase domain coarsening. *Acta Metall.* 27:1084–1095.

53. Saintillan, D., M. J. Shelley, and A. Zidovska. 2018. Extensile motor activity drives coherent motions in a model of interphase chromatin. *Proc. Natl. Acad. Sci. USA*. 115:11442–11447.

54. Zwicker, D., J. Baumgart, …, F. Jülicher. 2018. Positioning of particles in active droplets. *Phys. Rev. Lett.* 121:158102.

55. McCarty, J., K. T. Delaney, …, J. E. Shea. 2019. Complete phase diagram for liquid-liquid phase separation of intrinsically disordered proteins. *J. Phys. Chem. Lett.* 10:1644–1652.

56. Lázaro, G. R., I. Pagonabarraga, and A. Hernández-Machado. 2015. Phase-field theories for mathematical modeling of biological membranes. *Chem. Phys. Lipids.* 185:46–60.

57. Lázaro, G. R., I. Pagonabarraga, and A. Hernández-Machado. 2017. Elastic and dynamic properties of membrane phase-field models. *Eur. Phys. J. E Soft Matter.* 40:77.

58. Elliott, C. M., and B. Stinner. 2010. Modeling and computation of two phase geometric biomembranes using surface finite elements. *J. Comput. Phys.* 229:6585–6612.

59. Slaughter, A. E., J. W. Peterson, …, J. M. Miller. 2015. Continuous integration for concurrent MOOSE framework and application development on GitHub. *J. Open Res. Softw.* 3::e14.

60. Gaston, D. R., C. J. Permann, …, R. C. Martineau. 2015. Physics-based multiscale coupling for full core nuclear reactor simulation. *Ann. Nucl. Energy.* 84:45–54.

61. Ayachit, U. 2012. The Paraview Guide: A Parallel Visualization Application. Kitware Inc., Clifton Park, NY.

62. Larson, A. G., and G. J. Narlikar. 2018. The role of phase separation in heterochromatin formation, function, and regulation. *Biochemistry.* 57:2540–2548.

63. Chiang, M., D. Michieletto, …, T. Chandra. 2018. Lamina and heterochromatin direct chromosome organisation in senescence and progeria. *bioRxiv* https://doi.org/10.1101/468561.

64. Falk, M., Y. Feodorova, …, L. A. Mirny. 2019. Heterochromatin drives compartmentalization of inverted and conventional nuclei. *Nature.* 570:395–399.

65. Solovei, I., K. Thanisch, and Y. Feodorova. 2016. How to rule the nucleus: divide et impera. *Curr. Opin. Cell Biol.* 40:47–59.

66. Solovei, I., A. S. Wang, …, B. Joffe. 2013. LBR and lamin A/C sequentially tether peripheral heterochromatin and inversely regulate differentiation. *Cell.* 152:584–598.

67. Solovei, I., M. Kreysing, …, B. Joffe. 2009. Nuclear architecture of rod photoreceptor cells adapts to vision in mammalian evolution. *Cell.* 137:356–368.

68. Caragine, C. M., S. C. Haley, and A. Zidovska. 2018. Surface fluctuations and coalescence of nucleolar droplets in the human cell nucleus. *Phys. Rev. Lett.* 121:148101.

69. Chu, F. Y., S. C. Haley, and A. Zidovska. 2017. On the origin of shape fluctuations of the cell nucleus. *Proc. Natl. Acad. Sci. USA*. 114:10338–10343.

70. Gürsoy, G., Y. Xu, …, J. Liang. 2014. Spatial confinement is a major determinant of the folding landscape of human chromosomes. *Nucleic Acids Res.* 42:8223–8230.

71. Lukášová, E., A. Kovařík, and S. Kozubek. 2018. Consequences of lamin B1 and lamin B receptor downregulation in senescence. *Cells.* 7:E11.

72. Feric, M., N. Vaidya, …, C. P. Brangwynne. 2016. Coexisting liquid phases underlie nucleolar subcompartments. *Cell.* 165:1686–1697.

73. Gibbs, E. B., and R. W. Kriwacki. 2018. Linker histones as liquid-like glue for chromatin. *Proc. Natl. Acad. Sci. USA.* 115:11868–11870.

74. Maeshima, K., S. Ide, …, M. Sasai. 2016. Liquid-like behavior of chromatin. *Curr. Opin. Genet. Dev.* 37:36–45.

75. Iborra, F. J. 2007. Can visco-elastic phase separation, macromolecular crowding and colloidal physics explain nuclear organisation? *Theor. Biol. Med. Model.* 4:15.

76. Erdel, F., and K. Rippe. 2018. formation of chromatin subcompartments by phase separation. *Biophys. J.* 114:2262–2270.

77. Polovnikov, K. E., M. Gherardi, …, M. V. Tamm. 2018. Fractal folding and medium viscoelasticity contribute jointly to chromosome dynamics. *Phys. Rev. Lett.* 120:088101.

78. Socol, M., R. Wang, …, A. Bancaud. 2019. Rouse model with transient intramolecular contacts on a timescale of seconds recapitulates folding and fluctuation of yeast chromosomes. *Nucleic Acids Res.* 47:6195–6207.

Biophysical Journal, Volume *118*

Supplemental Information

Mesoscale Liquid Model of Chromatin Recapitulates Nuclear Order of Eukaryotes

Rabia Laghmach, Michele Di Pierro, and Davit A. Potoyan

Supporting Information for: "Mesoscale liquid model of chromatin recapitulates intra-nuclear order of eukaryotes."

Authors: Rabia Laghmach, Michele Di Pierro, Davit A. Potoyan

September 11, 2019

1 Supporting Information

1.1 Description of the MELON model for studying chromatin reorganization at nuclear scales

Here we explain in greater detail the physical set up and numerical implementation of the MELON framework to model the drosophila nucleus. In this framework, the state of the nucleus is resolved using several order parameters describing the local state of chromatin within a physical domain Ω. The nucleus is defined through the phase-field variable $\varphi_0(\mathbf{r},t)$ which takes 0 inside the nucleus and 1 outside with a smooth variation in-between the regions. The variable $\mathbf{r}$ is the spatial position and t is time. The nuclear envelope (membrane) is represented by a diffuse interfacial layer of the nucleus with a small thickness. The N chromosomal territories inside the nucleus are described by individual phase-field variables $(\{\phi_i(\mathbf{r},t)\}; i = 1,\cdots,N)$. The chromatin types A and B which form the euchromatin-heterochromatin territories are resolved by defining a field variable $\psi(\mathbf{r},t)$ which quantifies the epigenetic state of the chromosomal region. Each order parameter takes a constant value in its respective two coexisting phases such that it is 1 within its domain, 0 within all the other domains while varying smoothly between interfacial regions. The nucleus interface position is defined through an iso-contour given by $\Gamma_{\varphi_0}(t) = \{\mathbf{r} \in \Omega, \varphi_0(\mathbf{r},t) = 1/2\}$. For chromosome and heterochromatin interfaces positions are given by the iso-contours $\Gamma_{\phi_i,\psi}(t) = \{\mathbf{r} \in \Omega, \phi_i(\mathbf{r},t) = 1/2$ and $\psi(\mathbf{r},t) = 1/2\}$.

To investigate the micron scale fluid dynamics and pattern formation of epigenetically colored nuclear chromatin, we need to construct the local free energy functional based on different physical features of the system: phase separation, surface tension, volume constraints and specific interactions between different chromatin types. We start by introducing the fundamental Ginzburg-Landau free energy functional which describes the phase separation and the overall shape of multi-phase field variables:

$$F_B[\varphi_0,\{\phi_i\}_{i=1,\ldots,N},\psi] = \int_\Omega d\mathbf{\Omega}\left[f_{\text{coex}}(\varphi_0) + \frac{\epsilon^2_{\varphi_0}}{2}(\nabla\varphi_0)^2\right] + \sum_{i=1}^{N}\int_\Omega d\mathbf{\Omega}\left[f_{\text{coex}}(\phi_i) + \frac{\epsilon^2_{\phi}}{2}(\nabla\phi_i)^2\right] + \int_\Omega d\mathbf{\Omega}\left[f_{\text{coex}}(\psi) + \frac{\epsilon^2_{\psi}}{2}(\nabla\psi)^2\right] \quad (1)$$

where f_{coex} is the coexisting bulk free energy density and the gradient term represent a contribution to the surface energy of the bulk phases interface. The gradient parameters ϵ_{φ_0}, ϵ_ϕ and ϵ_ψ are controlling the thickness of the interfacial region as defined by the variables φ_0, ϕ_i and ψ respectively, and are taken to be small compared to the length-scale of the nucleus. The bulk free energy density has two minima centered at 0 and 1 each of which corresponds to equilibrium bulk phase. We choose the standard double-well potential to describe the coexisting bulk phases: $f_{\text{coex}}(\varphi_0) = \varphi_0^2(1-\varphi_0)^2/4$. The form of the coexistence function allows connecting the free energy profile of two bulk phases for each phase variable and makes finite contribution only to the interfacial energy. With this expression, the overall shape of the interfaces is governed only by the interfacial energies which penalize the movement of the interfaces. The coexistence function guarantees the attainment of stable diffuse interfaces separating the coexisting bulk phases. The minimization of the F_B gives the profile of the interface: $1/2\left[1-\tanh\left(r/2\sqrt{2}\epsilon_{\cdot}\right)\right]$ with thickness parameter $\epsilon_{\cdot}$ defined above for different interfaces. The motion of interfaces is governed not only by interfacial energy but also by local bulk driving force of the phase transition $\Delta f_{\text{bulk}}(\cdot)$, with $f_{\text{bulk}}(\cdot) = f_{\text{coex}}(\cdot) + \cdots$. We now turn to describing the energetic terms representing the bulk driving forces of the phase separation.

To generate the state of a nucleus which is fully occupied by chromosomal domains it is important to allow chromosomal territories to expand and contract in response to nuclear volume changes in a way a dense polymeric

solution would respond. In order to account for the constraints imposed by the nuclear volume we introduce a "growth" term of the global free energy functional F_G as follows:

$$F_G[\varphi_0, \{\phi_i\}_{i=1,\dots,N}, \psi] = \alpha_{Neq}\left[\overline{V}_N - V_N(t)\right]^2 + \alpha_N\left[V_N(t) - \sum_{i=1}^{N} V_i(t)\right]^2 + \\ +\alpha_V \sum_{i=1}^{N}\left[V_i(t) - \overline{V}_i(t)\right]^2 + \alpha_v \sum_{i=1}^{N}\left[v_i(t) - \overline{v}_i(t)\right]^2 \tag{2}$$

where V_N is the nuclear volume, α_{Neq}, α_N, α_V and α_v are positive coefficients. The first term accounts for the changes of nuclear volume during nuclear reorganization (growth or inversion) stage during which the nucleus evolves towards a new steady-state volume $\overline{V}_N$. The harmonic terms acting on volumes of chromosomal domains ensures that all the chromosomes fill the nuclear volume entirely V_N, with an additional volume constraints ensuring the proper ratio of heterochromatin to chromosome domains $\overline{v}_i$ and $\overline{V}_i$ respectively. Notice that the coefficients α_{Neq}, α_N, α_V and α_v control the kinetics of growth of different domains to reach the prescribed volumes because their respective driving forces are proportional to these parameters.

The volume of each chromosome denoted by V_i and their corresponding heterochromatin domain volume v_i are defined as the spatial integral of their interface profile described by the variables ϕ_i and ψ. This usual approximation of the volume will change the minima of f_{bulk} which corresponds to the equilibrium bulk phases. We thus adopt an interpolation function h to approximate the volumes for different compartments while keeping the positions of minima of f_{bulk} function at 0 and 1. The most frequently adopted polynomial function for calculations using diffuse interface methods [1] is: $h(\varphi_0) = \varphi_0^3(10 - 15\varphi_0 + 6\varphi_0^2)$. Therefore, we approximate the volumes for nucleus V_N, chromosomes V_i and heterochromatin domains v_i by:

$$V_N(t) = \int_\Omega d\mathbf{\Omega}\left[1 - h(\varphi_0)\right]; \quad V_i(t) = \int_\Omega d\mathbf{\Omega} h(\phi_i); \qquad v_i(t) = \int_\Omega d\mathbf{\Omega} h(\phi_i)h(\psi)$$

At this point, the free energy functional sketched above describes only the growth and shrinkage of chromosomal domains. To ensure that changes in volumes of chromosomes are coupled to each other we introduce additional energetic terms which penalize the overlap between chromatin domains during the process of nuclear volume change:

$$F_R[\varphi_0, \{\phi_i\}_{i=1,\dots,N}, \psi] = 4\beta_0 \sum_{i=1}^{N}\int_\Omega d\mathbf{\Omega} h(\varphi_0)\left(1 - h(\varphi_0)\right)h(\phi_i) + \\ \beta_\psi \int_\Omega d\mathbf{\Omega}\left[1 - \sum_{i=1}^{N} h(\phi_i)\right]h(\psi) + \beta_\phi \sum_{i\neq j}^{N}\int_\Omega d\mathbf{\Omega} h(\phi_i)h(\phi_j) \tag{3}$$

Coefficients β_0, β_ψ and β_ϕ are all positive constants in the model. The first term represents an energetic belt which surrounds the nucleus by restricting the movement of all chromosome territories within the nuclear envelope. In fact, this energy increases when the chromosome territories are near the nuclear envelope and thus penalize strongly the movement of at the peripheral regions of the nucleus. The second and third terms account for the excluded volume interactions between chromosome-chromosome territories and chromatin-heterochromatin domains. Thus, the chromosome territories cannot overlap and maintain their prescribed volume defined previously in F_G. The interaction between the heterochromatin and the lamina located at the nuclear envelope plays a crucial role in the nuclear organization and restructuring through the adhesion/desperation processes happening during the cell development. To account for the affinity of heterochromatin towards nuclear envelope, several formulations of adhesion could be developed as a function of corresponding phase-fields variables ψ and φ_0. Some of the commonly used formulations for adhesive interaction have used polynomial [2, 3] and exponential [3] forms. The adhesion energy depends on the distance of heterochromatin interface from the nuclear envelope. The form of interaction potential between heterochromatin and the nuclear envelope that we have used is the same one which was also used in many prior works of phase-field models [4, 5]:

$$F_I[\varphi_0, \psi] = \gamma \int_\Omega d\mathbf{\Omega}\nabla h(\varphi_0)\cdot\nabla h(\psi) \tag{4}$$

This form of the potential ensures that the adhesion energy is negative in the region of overlapping of the nuclear envelope and heterochromatin interfacial layer and zero elsewhere. Here the γ is a positive coefficient which quantifies the binding affinity of heterochromatin domains to nuclear Lamina.

The total free energy of the system that accounting all effect considered for the nature of intra-nuclear chromatin is expressed then as:

$$F[\varphi_0, \{\phi_i\}_{i=1,\dots,N}, \psi] = F_B + F_G + F_R + F_I \tag{5}$$

The dynamics of chromatin is described through the temporal evolution of the non-conserved order parameters following the Allen-Cahn kinetic equation [6] which is derived through minimization of the free energy functional [5]:

$$\frac{\partial \varphi_0}{\partial t} = -L_{\varphi_0}\frac{\delta F}{\delta \varphi_0}; \qquad \frac{\partial \phi_i}{\partial t} = -L_{\phi_i}\frac{\delta F}{\delta \phi_i}\bigg|_{(i=1,\dots,N)}; \qquad \frac{\partial \psi}{\partial t} = -L_{\psi}\frac{\delta F}{\delta \psi} + \eta_{\psi}(\mathbf{r},t) \tag{6}$$

where noise terms are defined via fluctuation-dissipation condition $\langle \eta_\psi(\mathbf{r},t)\,\eta_\psi(\mathbf{r}',t')\rangle = 2k_bTL_\psi\delta(\mathbf{r}-\mathbf{r}')\,\delta(t-t')$ with terms L_{φ_0}, L_{ϕ_i} and L_ψ being the mobility coefficients associated with their respective fields. The term η_ψ is added to the evolution equation of the phase-field ψ to account the thermal fluctuation effects of the heterochromatin region at the average time-scale. The amplitude of fluctuation is determined by the fluctuation-dissipation relation, which is related to the mobility coefficient L_ψ. By calculating the variational derivative of the total free energy functional F in [6], we get the system of relaxation equations:

$$\begin{aligned}\frac{\partial \varphi_0}{\partial t} = \quad & L_{\varphi_0}\Bigg(\epsilon_{\varphi_0}^2\nabla^2\varphi_0 - f'_{\text{coex}}(\varphi_0) - 2h'(\varphi_0)\Bigg\{2\beta_0\left(1-2h(\varphi_0)\right)\sum_{i=1}^{N}h(\phi_i) - \alpha_0\left[V_N(t) - \sum_{i=1}^{N}V_i(t)\right] \\ & -\frac{\gamma}{2}\nabla^2 h(\psi) + \alpha_4\left[\overline{V}_N - V_N(t)\right]\Bigg\}\Bigg)\end{aligned} \tag{7}$$

$$\begin{aligned}\frac{\partial \phi_i}{\partial t} = \quad & L_{\phi_i}\Bigg(\epsilon_{\phi}^2\nabla^2\phi_i - f'_{\text{coex}}(\phi_i) - 2h'(\phi_i)\Bigg\{\alpha_V\left[V_i(t) - \overline{V}_i(t)\right] - \alpha_0\left[V_N(t) - \sum_{i=1}^{N}V_i(t)\right] \\ & +\alpha_v\left[v_i(t) - \overline{v}_i(t)\right]h(\psi) + 2\beta_0 h(\varphi_0)\left(1-h(\varphi_0)\right) - \frac{\beta_\psi}{2}h(\psi) + \frac{\beta_\phi}{2}\left[\sum_{i=1}^{N}h(\phi_i) - h(\phi_i)\right]\Bigg\}\Bigg)\end{aligned} \tag{8}$$

$$\frac{\partial \psi}{\partial t} = L_\psi\left(\epsilon_\psi^2\nabla^2\psi - f'_{\text{coex}}(\psi) - h'(\psi)\left\{2\alpha_v\sum_{i=1}^{N}\left[v_i(t) - \overline{v}_i(t)\right]h(\phi_i) + \beta_\psi\left(1 - \sum_{i=1}^{N}h(\phi_i)\right) - \gamma\nabla^2 h(\varphi_0)\right\}\right) + \eta_\psi(\mathbf{r},t) \tag{9}$$

When the nuclear volume is constant $V_N(t) = \overline{V}_N$, the governing equations of chromatin dynamics [Eq 6] are reduced to [Eq 8, 9] which also makes the interfacial profile of nucleus independent of time: $\varphi_0(\mathbf{r},t) = \varphi_0(\mathbf{r}) = \frac{1}{2}\left\{1 - \tanh\left(r/2\sqrt{2}\epsilon_{\varphi_0}\right)\right\}$.

Finally, the equations governing chromatin dynamics are resolved in nondimensional form. For that we introduce the length-scale l and the time-scale t for dimensionlizing the equations. The length scale was set to $1\mu m$ and the mobility parameter was chosen to set the time length as a unit.

Numerical simulations and parameter setting:

Let consider the application of MELON framework to model drosophila nucleus with 8 chromosome territories. The governing equations of the chromatin dynamics are highly nonlinear. To solve the coupled non-dimensional equations resulting from minimization of the global free energy functional, we use a fully implicit finite element method combined with the preconditioned Jacobian Free Newton Krylov (JFNK) technique [7]. The development of the MELON framework and equations that are derived from it have been implemented in the MOOSE library [8, 9]: it's a massively parallel finite element open-source coded on C++ language which was builds using several high-performance computational libraries for solving nonlinear partial differential equations: MPI, LibMesh, PETSc. Once all the equations are transformed in the weak form to extract the residual vectors, we compute the solution of the phase field variables by using the different kernels implemented in Moose phase-field module. More details of the numerical implementation of the phase-field module are given in [10, 8].

The simulations were performed on a rectangular domain of dimensions $6\ \mu m \times 9\ \mu m$. A quadrilateral element with 4 nodes was used for domain meshing with the refinement. The total number of elements used for the fine mesh is 640000. The time step of integration Δt is fixed at 0.0025 [a.u.]. An elliptical nucleus is introduced in the center of computational domain in which the chromosomes and heterochromatin domains are randomly generated. The initial conditions to generate the conventional nuclear architecture are provided by a tanh-like function: $1/2\left[1 - \tanh\left(r/2\sqrt{2}\epsilon_.\right)\right]$. The geometries of different subdomains described by the phase-field variables $\varphi_0, \{\phi_i\}_{i=1,\dots,N}, and\, \psi$ have an elliptical shape where r represents the signed distance function. We use the steady-state of conventional architecture as an initial condition to study the nuclear reorganization process. For interface geometry of the nucleus, two cases have been considered in this work. With fixed nucleus volume: $\varphi_0(r)$ and with a dynamic relaxation of the nuclear interface through $\varphi_0(r,t)$ which remodels nuclear volume as function time until steady-state volume $\overline{V}_N$. When nuclear volume is kept constant, the nucleus interface is simulated by an elliptical shape in which the semi-major axes are fixed to $a = 2.5\,\mu m$ and the semi-minor axis to $b = 4\,\mu m$; thus the nuclear

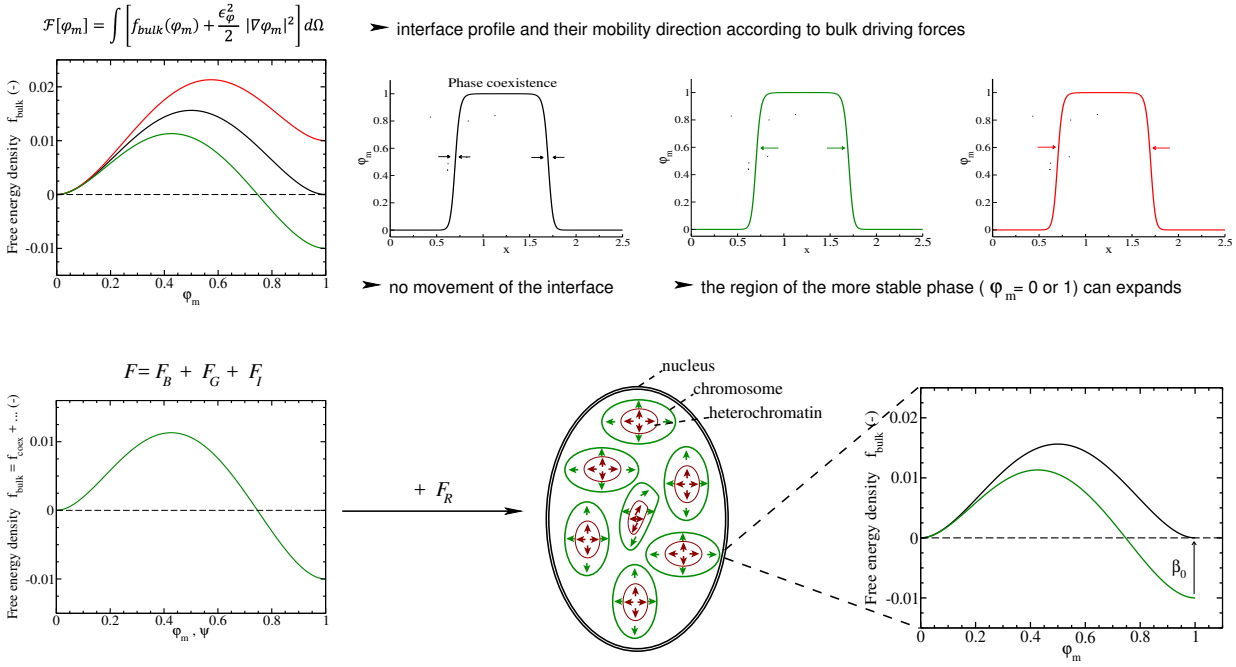

Figure 1: Illustration of MELON free energy terms for intra-nuclear chromatin dynamic. Shown are bulk free energy density as a function of the phase field variable ϕ_m and their corresponding interface profile. The relative position of the f_{bulk} indicates the phase transition direction.

volume is: $V_N = \pi ab = 31.416\,\mu m^2$. For volume remodeling simulations, we compute the temporal evolution of the nuclear volume through h-function as follows: $V_N(t) = \int_\Omega d\mathbf{\Omega}[1 - h(\varphi_0)]$. The mobility coefficient of the nuclear interface is linked to the volume reduction rate in the following way: $L_{\varphi_0} = (V_N(t_0) - \overline{V}_N)/((t_f - t_0) \times V_N(t_0))$, where the coefficient α_{Neq} (fixed at 2 for conventional architecture) controls the nuclear interface velocity . The mobility of chromosomal and heterochromatin compartments are set to be equal $L = L_\varphi = L_\psi$. Since this parameter fixes the inter and intra-chromosomal interface relaxation time: $\tau \propto L^{-1}$. The interface relaxation time τ is used to set the unit timescale for the kinetics of phase transitions. We note that the value of τ is naturally expected to be different for different developmental stages of the nucleus. For instance for the post-embryonic interphase of drosophila [11] we set $\tau \sim 0.005\,h$ while for studying long time senescence and nuclear inversion the time scale is calibrated to match different set of experiments [12] and corresponds to $\tau \sim 5\,h$.
The interfacial parameters $\epsilon_\varphi, \epsilon_\psi$ quantify thickness of inter and intra-chromosomal compartments respectively. These parameters can be estimated through the interfacial energies of chromosome territories and euchromatin-heterochromatin compartments. We estimate the interfacial parameters through the diffusion coefficient: $D_\varphi = L\,\epsilon_\varphi^2$ for chromosomes and $D_\psi = L\,\epsilon_\psi^2$ for the heterochromatin regions. By varying the interfacial parameters, we have investigated how the diffusion coefficient impact the nuclear architecture organization and chromatin dynamics. We estimate diffusion coefficients from long-time scale measurements of diffusion of chromosomal loci where clear diffusive behaviour is seen [13, 14]. In this study we have varied the diffusion coefficients wihtin a resonable range that accouts for cellular variablility. The range of values considered is D_ψ=[$0.003\,\mu m^2/h$, $0.004\,\mu m^2/h$, $0.008\,\mu m^2/h$] and D_φ=[$0.0015\,\mu m^2/h$, $0.001\,\mu m^2/h$]. The thickness of the diffuse interfacial layer of the nucleus, the heterochromatin and the chromosome compartments are all determined by $\kappa_. = 4\sqrt{2}\epsilon_. \tanh^{-1}(1 - 2\zeta)$ where ζ is set to 0.1. The specific values are, $\kappa_{\varphi_0} = 0.44\mu m$, $\kappa_\phi = 0.44\mu m, 0.538\mu m$ and $\kappa_\psi = 0.761\mu m, 0.88\mu m, 1.243\mu m$. The nondimensionalized parameters of the model such as the intensity of the energetic belt surrounding the nuclear envelope and the excluded volume interaction parameters are simply chosen to be strong enough to contain all the chromosome territories within the nucleus and restrict the overlap. The value of parameters are respectively set to $\beta_0 = 16.67$ and $\beta_\varphi = 40$ for all the simulations. The interaction range of heterochromatin regions has been varied within a range: $\beta_\psi = 0.1 - 0.4$ to investigate its impact on the degree of euchromatin-heterochromatin mixing. For nuclear reorganization simulations, the parameter β_ψ was fixed to 0.1. The computed values of the growing domains kinetic parameters are set as $\alpha_0 = 0.16$, and $\alpha_v = \alpha_V = 2$. The interaction parameter between heterochromatin and nuclear lamina is chosen to be the smaller value that allows maintaining the binding between them and is set as $\gamma = 0.009\,\mu m^2$. Euchromatin-heterochromatin interfacial fluctuation have been modeled as thermal noise with an amplitude set to $A = 2k_BTL$. Three values of fluctuation amplitude were considered here A=5, 10 and 15 which corresponding to the different effective temperatures in the nucleus.

Table 1: Fit settings used to extract the characteristic time (or relaxation time). Notice that the time necessary to reach the equilibrium state can be evaluated approximately to 3τ

	Final volume	function used for fit	a(μm)	b	$\tau(h)$
Nucleus			35.6931	0.11043	165.058
Chromosomes	110%	$a(1 - bexp(-t/\tau))$	35.043	0.115398	166.021
Heterochromatin			10.674	0.129893	147.994
Nucleus			16.0959	0.969034	295.307
Chromosomes	50%	$a(1 + bexp(-t/\tau))$	15.3689	1.03216	296.809
Heterochromatin			4.77723	0.9523	303.584
Nucleus			12.7916	1.47789	323.406
Chromosomes	40%	$a(1 + bexp(-t/\tau))$	12.0589	1.59465	324.675
Heterochromatin			3.77556	1.47166	331.641

Data Analysis: Kinetic aspects

The density of the heterochromatin at the i-th chromosome can be expressed as: $\rho_i(t) = v_i(t)/V_i(t)$. Thus, the associated euchromatin density is evaluated as $1 - \rho_i(t)$.
The density of the heterochromatin in cell's nucleus: $\rho(t) = v(t)/V(t)$

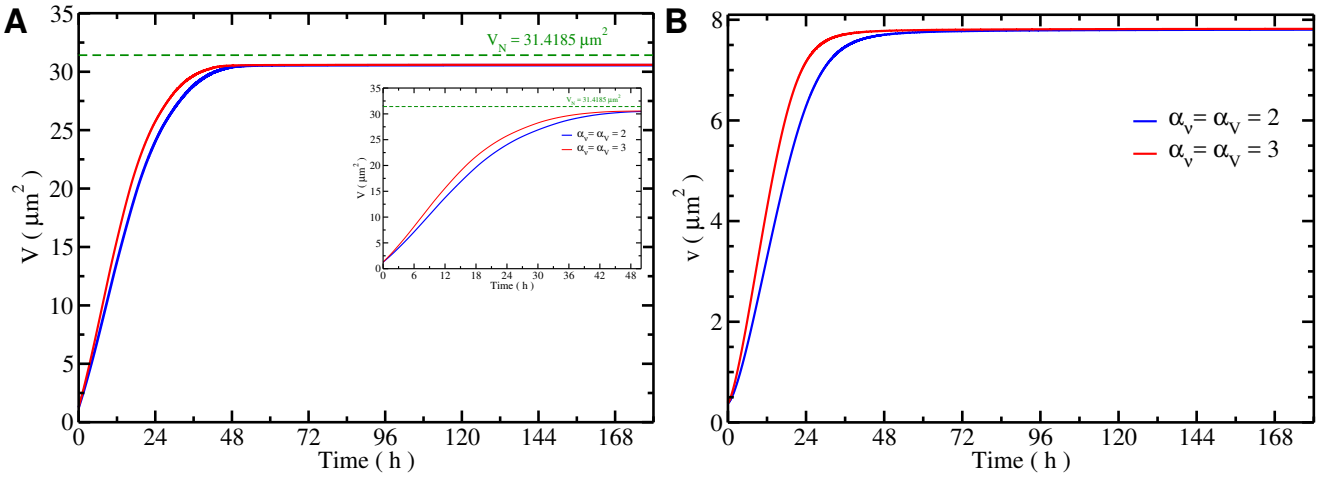

Figure 2: Temporal evolution of the overall chromosome (fig. a)) and heterochromatin (fig. b)) volumes in the cell's nucleus, without binding affinity with heterochromatin domain, for two different values of coefficient α_v and α_V.

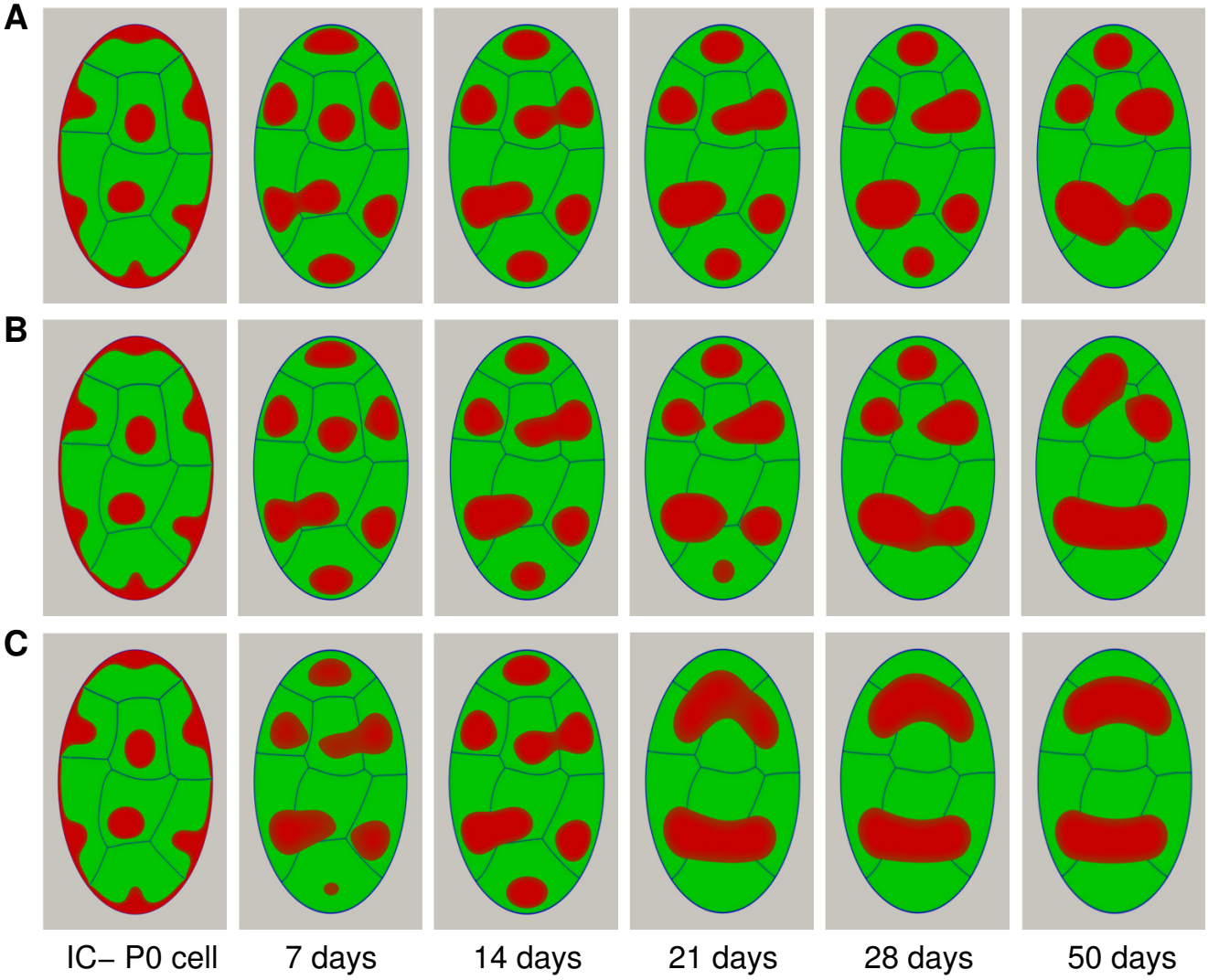

Figure 3: Effect of heterochromatin diffusion coefficient on nuclear architecture reorganization with a fixed cell's nucleus volume. The architecture obtained for a low diffusion coefficient $\epsilon_\psi^2 = 0.015\mu m^2$ is reported in fig a) and $0.02\mu m^2$ in fig. b), while for higher value $\epsilon_\psi^2 = 0.04\mu m^2$ is reported in fig. c). The heterochromatin density in cell's nucleus is fixed to 30%. The other parameters used: $\epsilon_\varphi^2 = 0.005\mu m^2$, $\beta_0 = 16.67$, $\beta_\varphi = 40$, $\beta_\psi = 0.1$, $\alpha_0 = 0.16$, and $\alpha_v = \alpha_V = 2$.

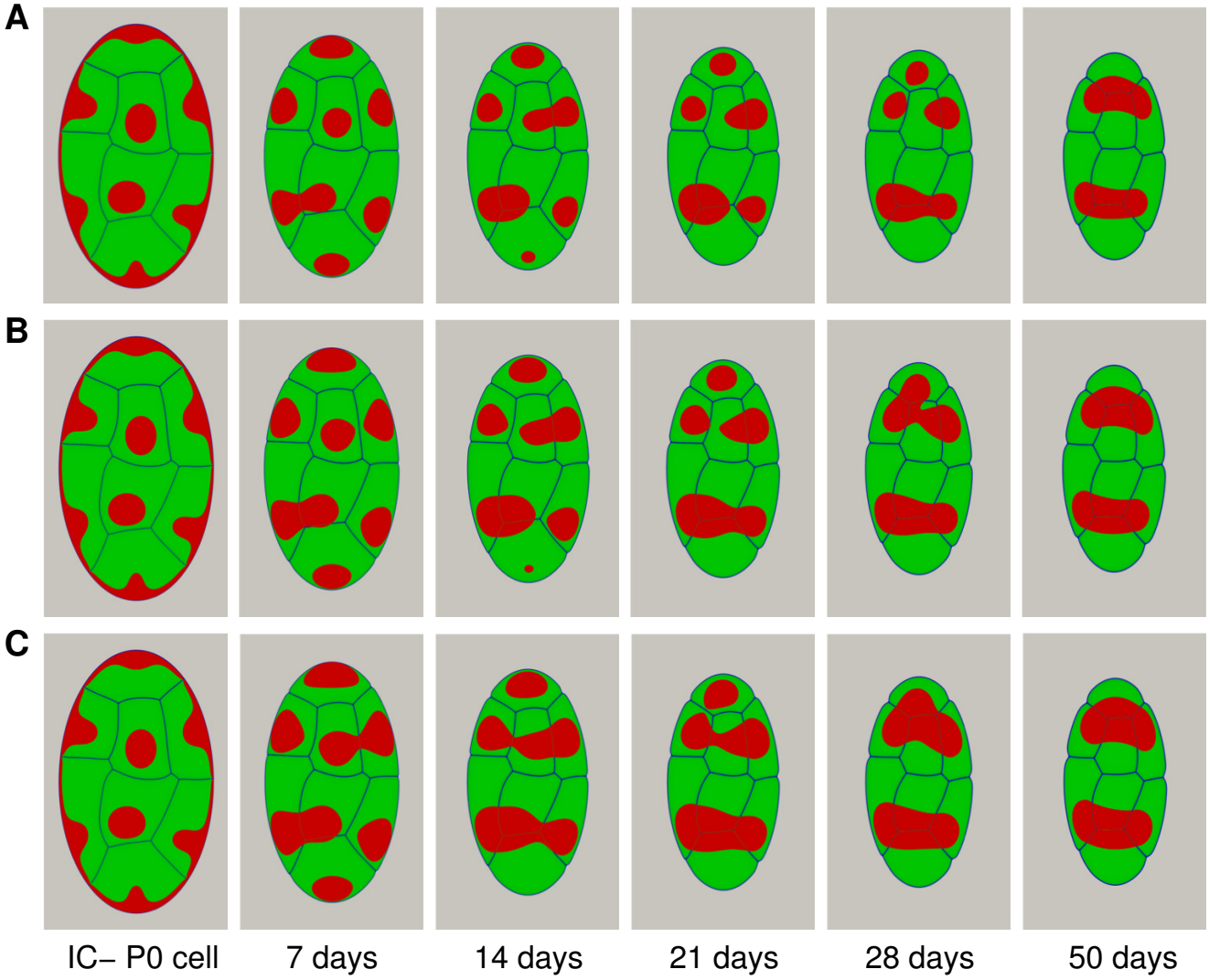

Figure 4: Effect of heterochromatin density in cell's nucleus on nuclear architecture reorganization. The architecture organization for a low density ($\rho = 25\%$) is reported in fig. a) and ($\rho = 30\%$) in fig. b) while for high value ($\rho = 35\%$) is reported in fig. c). The other parameters used: $\epsilon_\varphi^2 = 0.005$, $\epsilon_\psi^2 = 0.02$ $\beta_0 = 16.67$, $\beta_\varphi = 40$, $\beta_\psi = 0.1$, $\alpha_0 = 0.16$ and $\alpha_v = \alpha_V = 2$.

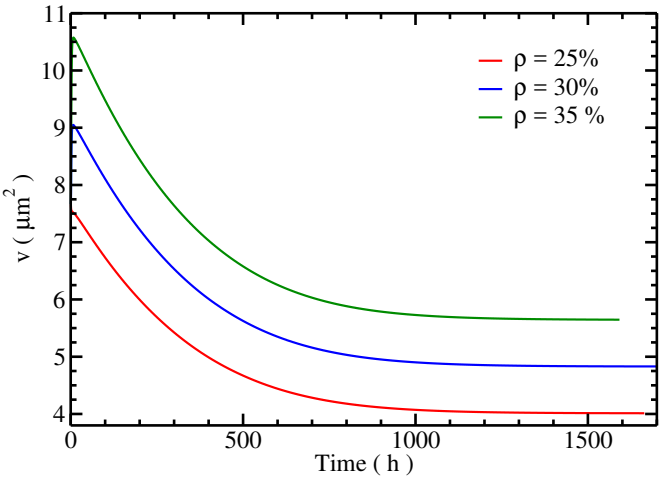

Figure 5: Temporal evolution of heterochromatin volume during the reorganization of nuclear architecture for two different value of heterochromatin density in the cell's nucleus (relaxation of heterochromatin domain: for $\rho = 25\%$ we found $a = 3.94977\mu m^2$, $b = 0.967667$ and $\tau = 305.096h^{-1}$; for $\rho = 30\%$ $a = 4.77723\mu m^2$, $b = 0.952299$ and $\tau = 303.586h^{-1}$, and we found $a = 5.53373\mu m^2$, $b = 0.957598$ and $\tau = 315.993h^{-1}$ for $\rho = 35\%$).

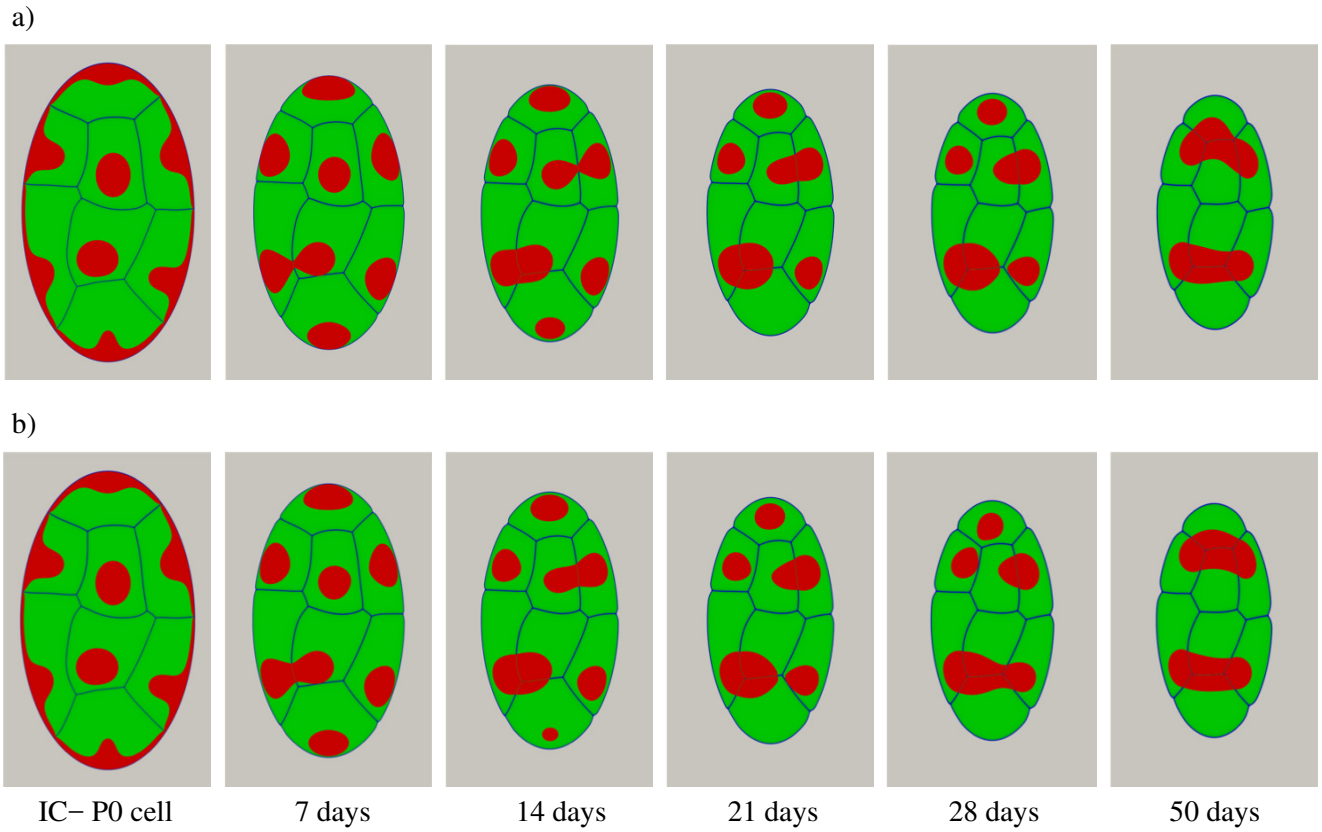

Figure 6: Effect of the heterochromatin diffusion coefficient on the reorganization of nuclear architecture accompanied by a change in the nuclear volume to reach 50% of its initial volume. The architecture organization for a low diffusion coefficient ($\epsilon^2_\psi = 0.015\,\mu m^2$) is reported in fig. a) while for high value ($\epsilon^2_\psi = 0.02\,\mu m^2$) is reported in fig. b). The other parameters used: $\epsilon^2_\varphi = 0.005$, $\beta_0 = 16.67$, $\beta_\varphi = 40$, $\beta_\psi = 0.1$, $\alpha_0 = 0.16$, $\alpha_v = \alpha_V = 2$ and $\rho = 30\%$.

References

[1] A. Karma and W.-J. Rappel, "Quantitative phase-field modeling of dendritic growth in two and three dimensions," *Phys. Rev. E*, vol. 57, pp. 4323–4349, Apr 1998.

[2] U. Seifert, "Adhesion of vesicles in two dimensions," *Phys. Rev. A*, vol. 43, pp. 6803–6814, Jun 1991.

[3] J. Zhang, S. Das, and Q. Du, "A phase field model for vesicle–substrate adhesion," *Journal of Computational Physics*, vol. 228, no. 20, pp. 7837 – 7849, 2009.

[4] M. Nonomura, "Study on multicellular systems using a phase field model," *PloS one*, vol. 7, no. 4, p. e33501, 2012.

[5] S. S. Lee, S. Tashiro, A. Awazu, and R. Kobayashi, "A new application of the phase-field method for understanding the mechanisms of nuclear architecture reorganization," *J. Math. Biol.*, 2017.

[6] S. M. Allen and J. Cahn, "Microscopic theory for antiphase boundary motion and its application to antiphase domain coarsening," *Acta. Metall.*, vol. 27, p. 1084, 1979.

[7] D. Knoll and D. Keyes, "Jacobian-free newton–krylov methods: a survey of approaches and applications," *Journal of Computational Physics*, vol. 193, no. 2, pp. 357 – 397, 2004.

[8] A. E. Slaughter, J. W. Peterson, D. R. Gaston, C. J. Permann, D. Andrs, and J. M. Miller, "Continuous integration for concurrent moose framework and application development on github," *Journal of Open Research Software*, vol. 3, 11 2015.

[9] D. R. Gaston, C. J. Permann, J. W. Peterson, A. E. Slaughter, D. Andrš, Y. Wang, M. P. Short, D. M. Perez, M. R. Tonks, J. Ortensi, L. Zou, and R. C. Martineau, "Physics-based multiscale coupling for full core nuclear reactor simulation," *Annals of Nuclear Energy*, vol. 84, pp. 45–54, 2015.

[10] R. M. Tonks, D. Gaston, P. C. Millett, D. Andrs, and P. Talbot, "An object-oriented finite element framework for multiphysics phase field simulations," *Computational Materials Science*, vol. 51, pp. 20–29, 2012.

[11] B. A. Edgar and P. H. O'Farrell, "The three postblastoderm cell cycles of drosophila embryogenesis are regulated in g2 by string," *Cell*, vol. 62, no. 3, pp. 469–480, 1990.

[12] I. Solovei, M. Kreysing, C. Lanctôt, S. Kösem, L. Peichl, T. Cremer, J. Guck, and B. Joffe, "Nuclear architecture of rod photoreceptor cells adapts to vision in mammalian evolution," *Cell*, vol. 137, pp. 356–368, Apr. 2009.

[13] I. Bronstein, Y. Israel, E. Kepten, S. Mai, Y. Shav-Tal, E. Barkai, and Y. Garini, "Transient anomalous diffusion of telomeres in the nucleus of mammalian cells," *Physical review letters*, vol. 103, no. 1, p. 018102, 2009.

[14] H. Hajjoul, J. Mathon, H. Ranchon, I. Goiffon, J. Mozziconacci, B. Albert, P. Carrivain, J.-M. Victor, O. Gadal, K. Bystricky, *et al.*, "High-throughput chromatin motion tracking in living yeast reveals the flexibility of the fiber throughout the genome," *Genome research*, 2013.